The corepressors GPS2 and SMRT control enhancer and silencer remodeling via eRNA transcription during inflammatory activation of macrophages

Zhiqiang Huang, Ning Liang, Saioa Goñi, Anastasios Damdimopoulos, Cheng Wang, Raphaelle Ballaire, Jennifer Jager, Henri Niskanen, Hongya Han, Tomas Jakobsson, et al.

▶ **To cite this version:**

Zhiqiang Huang, Ning Liang, Saioa Goñi, Anastasios Damdimopoulos, Cheng Wang, et al.. The corepressors GPS2 and SMRT control enhancer and silencer remodeling via eRNA transcription during inflammatory activation of macrophages. Molecular Cell, 2021, 10.1016/j.molcel.2020.12.040 . hal-03124222

HAL Id: hal-03124222

https://hal.sorbonne-universite.fr/hal-03124222

Submitted on 28 Jan 2021

HAL is a multi-disciplinary open access archive for the deposit and dissemination of scientific research documents, whether they are published or not. The documents may come from teaching and research institutions in France or abroad, or from public or private research centers.

L'archive ouverte pluridisciplinaire **HAL**, est destinée au dépôt et à la diffusion de documents scientifiques de niveau recherche, publiés ou non, émanant des établissements d'enseignement et de recherche français ou étrangers, des laboratoires publics ou privés.

Molecular Cell

Article

The corepressors GPS2 and SMRT control enhancer and silencer remodeling via eRNA transcription during inflammatory activation of macrophages

Graphical Abstract

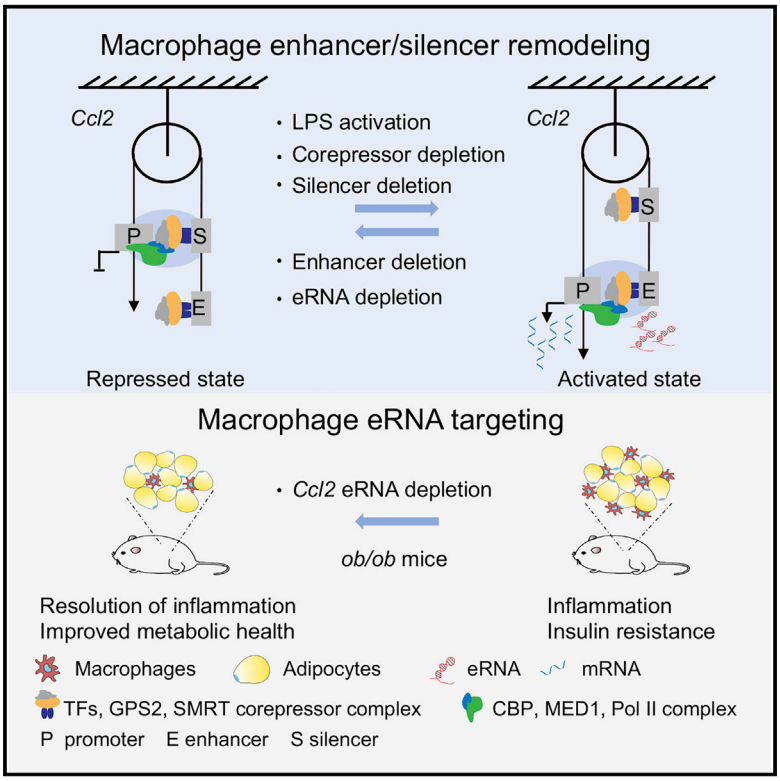

Highlights

- Corepressor recruitment is a genome-wide feature of inflammatory enhancers
- Corepressors control enhancer-silencer-promoter looping within the *Ccl2* TAD
- Corepressors antagonize eRNA transcription and CBP-mediated H3K27 acetylation
- *Ccl2* eRNA depletion in *ob/ob* mice supports eRNA function and targeting options

Authors

Zhiqiang Huang, Ning Liang, Saioa Goñi, ..., Minna U. Kaikkonen, Rongrong Fan, Eckardt Treuter

Correspondence

rongrong.fan@ki.se (R.F.), eckardt.treuter@ki.se (E.T.)

In Brief

Huang et al. dissect epigenetic mechanisms underlying the anti-inflammatory action of macrophage corepressors. By studying chromatin structure and histone modifications, transcription factor and coregulator dynamics, and eRNA transcription at the mouse *Ccl2* locus, they uncover a role of corepressors in controlling enhancer and silencer remodeling linked to inflammatory gene expression.

Huang et al., 2021, Molecular Cell *81*, 1–16
March 4, 2021 © 2020 Elsevier Inc.
https://doi.org/10.1016/j.molcel.2020.12.040

CellPress

Please cite this article in press as: Huang et al., The corepressors GPS2 and SMRT control enhancer and silencer remodeling via eRNA transcription during inflammatory activation of macrophages, Molecular Cell (2020), https://doi.org/10.1016/j.molcel.2020.12.040

Molecular Cell

CellPress

Article

The corepressors GPS2 and SMRT control enhancer and silencer remodeling via eRNA transcription during inflammatory activation of macrophages

Zhiqiang Huang,[1] Ning Liang,[1] Saioa Goñi,[1,10] Anastasios Damdimopoulos,[1] Cheng Wang,[2] Raphaelle Ballaire,[3] Jennifer Jager,[4,11] Henri Niskanen,[5,12] Hongya Han,[6] Tomas Jakobsson,[7] Adrian P. Bracken,[2] Myriam Aouadi,[4,8] Nicolas Venteclef,[9] Minna U. Kaikkonen,[5] Rongrong Fan,[1,*] and Eckardt Treuter[1,13,*]

[1]Department of Biosciences and Nutrition, Karolinska Institutet, 14183 Huddinge, Sweden
[2]Smurfit Institute of Genetics, Trinity College Dublin, Dublin 2, Ireland
[3]Inovarion, 75005 Paris, France
[4]Department of Medicine, Integrated Cardio Metabolic Centre (ICMC), Karolinska Institutet, 14152 Huddinge, Sweden
[5]A.I. Virtanen Institute for Molecular Sciences, University of Eastern Finland, PO Box 1627, 70211 Kuopio, Finland
[6]Department of Medicine, Centre for Hematology and Regenerative Medicine (HERM), Karolinska Institutet, 14183 Huddinge, Sweden
[7]Department of Laboratory Medicine, Karolinska Institutet, Division of Clinical Chemistry, Karolinska University Hospital, 14186 Huddinge, Sweden
[8]Department of Medicine, Centre for Infectious Medicine (CIM), Karolinska Institutet, 14152 Huddinge, Sweden
[9]Centre de Recherche des Cordeliers, INSERM, Université de Paris, Sorbonne Université, IMMEDIAB Laboratory, 75006 Paris, France
[10]Present address: Biochemistry and Molecular Biology Area, Department of Health Sciences, Public University of Navarra, 31008 Pamplona, Spain
[11]Present address: Université Côte d'Azur, INSERM, Centre Méditerranéen de Médecine Moléculaire (C3M), Team Cellular and Molecular Pathophysiology of Obesity and Diabetes, 06204 Nice, France
[12]Present address: Department of Genome Regulation, Max Planck Institute for Molecular Genetics, 14195 Berlin, Germany
[13]Lead contact
*Correspondence: rongrong.fan@ki.se (R.F.), eckardt.treuter@ki.se (E.T.)
https://doi.org/10.1016/j.molcel.2020.12.040

SUMMARY

While the role of transcription factors and coactivators in controlling enhancer activity and chromatin structure linked to gene expression is well established, the involvement of corepressors is not. Using inflammatory macrophage activation as a model, we investigate here a corepressor complex containing GPS2 and SMRT both genome-wide and at the *Ccl2* locus, encoding the chemokine CCL2 (MCP-1). We report that corepressors co-occupy candidate enhancers along with the coactivators CBP (H3K27 acetylase) and MED1 (mediator) but act antagonistically by repressing eRNA transcription-coupled H3K27 acetylation. Genome editing, transcriptional interference, and cistrome analysis reveals that apparently related enhancer and silencer elements control *Ccl2* transcription in opposite ways. 4C-seq indicates that corepressor depletion or inflammatory signaling functions mechanistically similarly to trigger enhancer activation. In *ob/ob* mice, adipose tissue macrophage-selective depletion of the *Ccl2* enhancer-transcribed eRNA reduces metaflammation. Thus, the identified corepressor-eRNA-chemokine pathway operates *in vivo* and suggests therapeutic opportunities by targeting eRNAs in immuno-metabolic diseases.

INTRODUCTION

The plasticity of macrophages in response to extracellular signals relies on rapid and reversible chromatin remodeling events coupled with transcriptional changes to control gene expression patterns (Glass and Natoli, 2016; Kuznetsova et al., 2020; Russell et al., 2019). These changes are coordinated by hierarchical networks of transcription factors (TFs) and coregulators, which cooperate to modify chromatin and to communicate with the basal transcription machinery, including RNA polymerase II (Pol II) (Heinz et al., 2010; Kaikkonen et al., 2013; Lam et al., 2013; Link et al., 2018; Romanoski et al., 2015). Although there are many candidate coactivators or corepressors involved in the control of inflammatory gene expression in macrophages, recent studies have highlighted the particular importance of an anti-inflammatory corepressor sub-complex containing the core subunits GPS2 and SMRT (hereafter referred to as GPS2 complex) (Barish et al., 2012; Fan et al., 2016; Huang et al., 2019b; Oberoi et al., 2011; Treuter et al., 2017), distinct from the pro-inflammatory NCOR-HDAC3 sub-complex (Emmett

Please cite this article in press as: Huang et al., The corepressors GPS2 and SMRT control enhancer and silencer remodeling via eRNA transcription during inflammatory activation of macrophages, Molecular Cell (2020), https://doi.org/10.1016/j.molcel.2020.12.040

and Lazar, 2019; Li et al., 2013; Mullican et al., 2011). Genome-wide transcriptome profiling of wild-type (WT) versus macrophage-specific *Gps2* knockout (KO) mice has revealed that expression of *Ccl2*, encoding C-C motif chemokine CCL2 (alias MCP-1 [monocyte chemoattractant protein-1]), is among the major inflammatory target genes that are repressed by the GPS2 complex in different macrophage populations. In humans with obesity and type 2 diabetes, *GPS2* expression in adipose tissue macrophages and blood monocytes inversely correlates with the expression of *CCL2* (Fan et al., 2016). Our previous cistrome and epigenome profiling has revealed that the GPS2 complex occupies a majority of H3K27ac-marked macrophage enhancers (Fan et al., 2016). This includes several enhancers that potentially control the expression of *Ccl2* but that have not yet been further characterized.

Enhancers are *cis*-regulatory elements of the epigenome that are located distally to the transcription start sites (TSSs) and function as binding sites for TFs and coregulators to transform signals from the cellular microenvironment into altered gene expression. Genome-wide studies suggest that one gene or co-regulated gene cluster (e.g., the *Ccl2* locus) is controlled by multiple enhancers (Andersson et al., 2014; Andersson and Sandelin, 2020; Osterwalder et al., 2018), but whether they all are uniquely required or act in part redundant has not yet been elucidated in the context of inflammatory gene expression. The field has defined key features of enhancers (Andersson and Sandelin, 2020; Cramer, 2019; Gasperini et al., 2020; Madsen et al., 2020; Partridge et al., 2020; van Steensel and Furlong, 2019), such as open chromatin, presence of TFs, MED1 (mediator), CBP/p300, H3K27ac, eRNA transcription, and promoter looping. However, corepressors are commonly not integrated into recent models of enhancer function, despite growing evidence that they co-occupy enhancers along with the above factors (Coppo et al., 2016; Czimmerer et al., 2018; Fan et al., 2016; Hatzi et al., 2013; Huang et al., 2019b; Kim et al., 2018; Li et al., 2013; Papachristou et al., 2018; Siersbæk et al., 2017; Treuter et al., 2017). This becomes highly relevant in light of recent studies describing *cis*-regulatory elements that seemingly share features with enhancers but act as silencers to repress transcription of linked genes (Doni Jayavelu et al., 2020; Gisselbrecht et al., 2020; Huang et al., 2019a; Ngan et al., 2020; Pang and Snyder, 2020). How these silencers communicate with enhancers and whether corepressor binding is a distinctive feature of such silencers has not yet been addressed.

The function of enhancers and silencers involves dynamic three-dimensional (3D) chromatin structure changes, which facilitate direct interactions with promoters through looping structures within defined topologically associating domains (TADs) (Kim and Shendure, 2019; Robson et al., 2019; van Steensel and Furlong, 2019). In contrast to static pre-established TADs formed by CTCF/cohesion (Hanssen et al., 2017; Jin et al., 2013), the formation of sub-TADs and intra-TAD enhancer-promoter loops is more tightly linked to changes in gene expression and can be dynamically regulated by CTCF/cohesin, YY1, nuclear receptors, and inflammatory TFs (Brown et al., 2014; Daniel et al., 2014; Hsieh et al., 2020; Kim et al., 2018; Krietenstein et al., 2020; Phanstiel et al., 2017; Ren et al., 2017; Weintraub et al., 2017). Of particular relevance appear AP-1 family members, including c-Jun and JunB, which are enriched at inflammatory enhancers (Fonseca et al., 2019; Phanstiel et al., 2017; Wolter et al., 2008; Vangala et al., 2020) and which are key target TFs of the GPS2 complex in macrophages (Fan et al., 2016; Treuter et al., 2017). Compared with the evidence supporting the critical role of TFs and coactivators in intra-TAD enhancer-promoter looping linked to inflammatory gene expression in macrophages, the mechanistic involvement of silencer elements and corepressors remains to be characterized.

Enhancer activity corelates with the transcription of non-coding enhancer RNAs (eRNAs) (Andersson and Sandelin, 2020; Henriques et al., 2018; Kaikkonen and Adelman, 2018; Kaikkonen et al., 2013; Lai et al., 2020; Lam et al., 2013; Lee and Mendell, 2020). Although it has remained challenging to distinguish between the function of eRNAs and the process of enhancer transcription, there is *in vitro* evidence that eRNAs bind to CBP/p300 to modulate their histone acetyltransferase activity (Bose et al., 2017). As CBP/p300 are the major H3K27 acetylases at enhancers (Raisner et al., 2018), there could be a functional link to eRNA transcription. Interestingly, GPS2 depletion increases H3K27ac levels at macrophage enhancers, which does not involve HDAC3 (Fan et al., 2016), suggesting a functional link to CBP/p300 and perhaps eRNA transcription.

In this study, we address these issues by characterizing the role of the GPS2 complex in controlling inflammatory gene expression in mouse macrophages, with an emphasis on the regulation of *Ccl2*. We provide evidence that GPS2 and SMRT prevent enhancer activation, which involves intra-TAD re-arrangements of promoter contacts with silencer and enhancer. We show further that these corepressors repress eRNA transcription and antagonize CBP-dependent H3K27 acetylation at enhancers. Finally, we demonstrate that the *in vivo* antisense targeting of a GPS2 complex-repressed *Ccl2* eRNA in adipose tissue macrophages of obese (*ob/ob*) mice can partially reverse metaflammation and insulin resistance, highlighting the *in vivo* potential of therapeutically targeting inflammatory enhancers.

RESULTS

Identification of *Ccl2* enhancer and silencer

To compare the genome-wide chromatin recruitment of the GPS2 corepressor complex to known enhancer marks in macrophages, we performed chromatin immunoprecipitation sequencing (ChIP-seq) for GPS2 along with H3K27ac, the macrophage lineage-determining TF PU.1, and the coactivators MED1 and CBP in the mouse macrophage RAW264.7 cell line (hereafter referred to as RAW cells). Genome-wide analysis revealed that GPS2 chromatin binding largely overlapped with MED1 and CBP both in basal condition (Figure 1A) and upon treatment with lipopolysaccharide (LPS; a TLR4 ligand) (Figure S1A). Although GPS2 was localized in both proximal (promoter) and distal (enhancer) regions along with H3K27ac, further analysis of its functional recruitment revealed that GPS2 bound more abundantly to enhancers than to promoters of repressed genes (Figure 1B). As MED1 marks also super-enhancers, we ranked the GPS2 peaks along with CBP and MED1 and identified the *Ccl2* enhancer region as a super-enhancer (Figure S1B).

Please cite this article in press as: Huang et al., The corepressors GPS2 and SMRT control enhancer and silencer remodeling via eRNA transcription during inflammatory activation of macrophages, Molecular Cell (2020), https://doi.org/10.1016/j.molcel.2020.12.040

CellPress

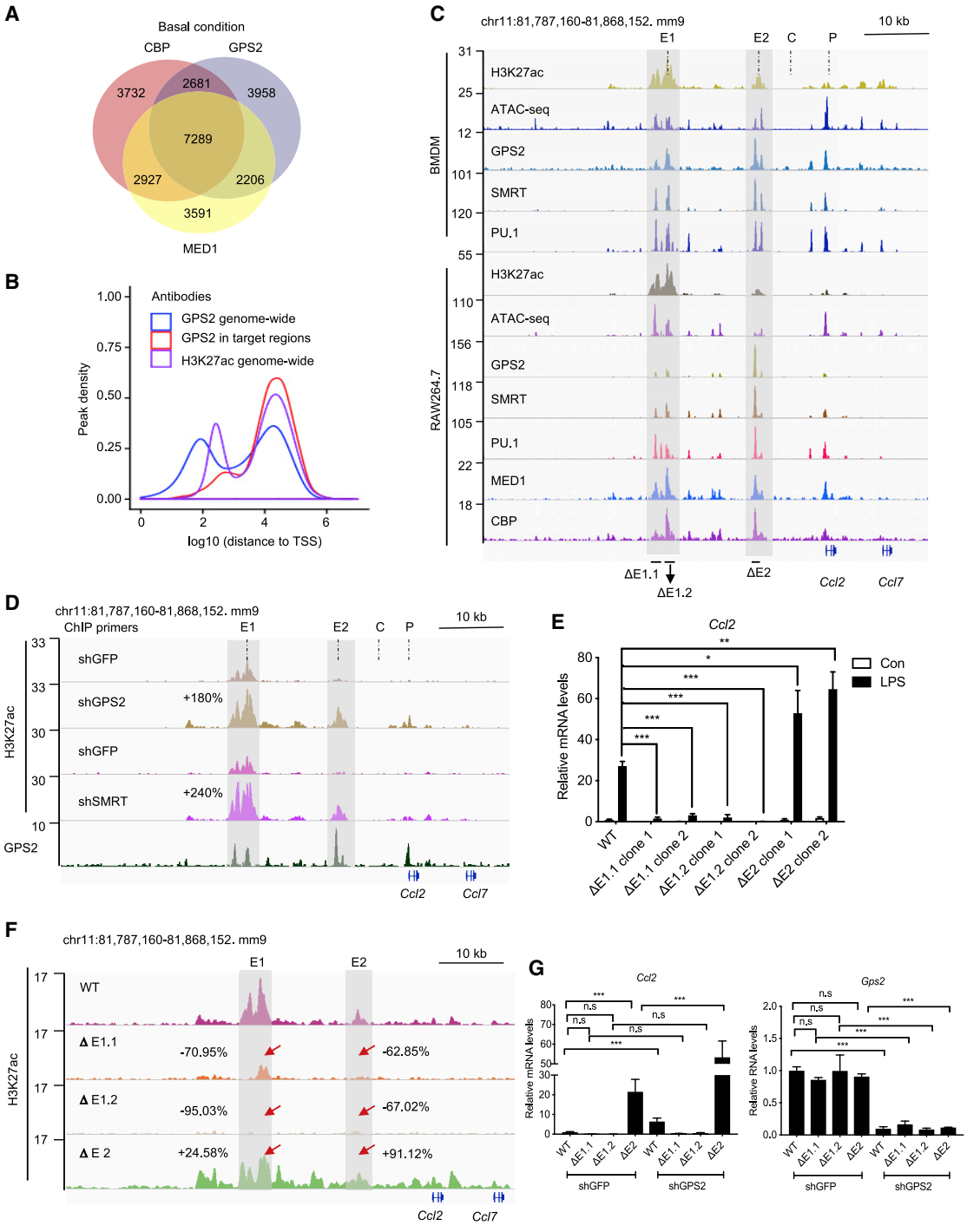

Figure 1. Mapping of GPS2/MED1/CBP/H3K27ac-positive macrophage enhancers and functional dissection at the *Ccl2* locus

(A) Venn diagram of common GPS2, CBP, and MED1 peaks as determined using ChIP-seq in RAW cells (basal condition).

(B) Density plot indicating peak densities in relation to distance to the transcription start sites (TSSs). The blue line represents all genome-wide GPS2 peaks, the purple line represents all genome-wide H3K27ac peaks, and the red line represents all genome-wide H3K27ac peaks that significantly changed upon GPS2 depletion. The x axis indicates the distance of individual peaks to the TSS of the closest annotated genes, and the y axis indicates the peak density, corresponding to the relative occupancy of GPS2 and H3K27ac across the genome.

(C) Genome Browser tracks representing the distribution of H3K27ac, open chromatin, TFs, and coregulators across the *Ccl2* locus in BMDMs and RAW cells. The BMDM data were obtained from the Gene Expression Omnibus (GEO) database for H3K27ac (GEO: GSM1631858), PU.1 (GEO: GSM1533888), GPS2 (GEO: GSM1631866), SMRT (GEO: GSM665925), and ATAC-seq (GEO: GSM2974654). The ChIP-seq and ATAC-seq data in RAW cells were generated in this study.

(legend continued on next page)

Please cite this article in press as: Huang et al., The corepressors GPS2 and SMRT control enhancer and silencer remodeling via eRNA transcription during inflammatory activation of macrophages, Molecular Cell (2020), https://doi.org/10.1016/j.molcel.2020.12.040

We specifically looked into the organization of the *Ccl2* locus as it is one of the most relevant GPS2-repressed genes in macrophages (Fan et al., 2016). We mapped the *Ccl2* super-enhancer in both bone marrow-derived macrophages (BMDMs) and RAW cells using ChIP-seq. Co-occupancy of GPS2 and SMRT, H3K27ac, MED1, CBP, and PU.1 identified two major enhancer clusters (Figure 1C). Both clusters were located in open chromatin regions identified using assay for transposase-accessible chromatin using sequencing (ATAC-seq) (Figure 1C). We then performed H3K27ac ChIP-seq in both GPS2 and SMRT-knockdown RAW cells (Figure 1D). Genome-wide analysis revealed that more than 70% of the altered H3K27ac signals at target genes were co-regulated by GPS2 and SMRT (Figure S1C). Re-analysis of published RNA sequencing (RNA-seq) data in WT versus GPS2-KO RAW cells (Huang et al., 2019b) confirmed that *Ccl2* is among these most significantly upregulated target genes (Figure S1D) and that this regulation is conserved between RAW cells and BMDMs (Fan et al., 2016). GPS2 and SMRT knockdown increased H3K27ac at both enhancers and promoter of *Ccl2* at basal condition, consistent with gene expression changes (Figures 1D, S1E, and S1F), while nearby upstream genes were not affected (Figure S1G). Notably, knockdown of SMRT completely abrogated GPS2 recruitment at the *Ccl2* locus and genome-wide (Figures S1H and S1I). This suggests that SMRT acts as the primary chromatin docking site of this corepressor sub-complex in macrophages, while GPS2 acts modulatory.

Further dissection of the two major *Ccl2* enhancer clusters revealed their distinct function. We used CRISPR-Cas9 to delete the regions around the TF/coregulator binding centers (460 bp for the distal E1.1, 565 bp for the proximal E1.2, and 621 bp for E2) in RAW cells (for exact locations of the deleted regions, see STAR methods). Strikingly, we found that deletion of the distal enhancer (E1.1 or E1.2) abolished LPS-induced *Ccl2* and *Ccl7* expression (both genes share promoters), while removal of the proximal enhancer (E2) showed the opposite effect (Figures 1E and S1J). This regulation was gene specific, as the neighboring gene *Asic2* was not affected (Figure S1J). As enhancer activation is regulated by multiple TFs that may differentially respond to individual inflammatory signals, we tested the responses of the enhancer-deleted RAW cells to KLA (TLR4), IFNλ (STAT1), TPA (AP-1), IL-4 (STAT6), TNF-α (NF-κB) and IL-6 (STAT1/3, AP-1). We observed that the opposite function of E1 and E2 was universal and stimulus independent, as all signal responses were abrogated in E1-deleted cells but elevated in E2-deleted cells (Figure S1K).

We next performed H3K27ac ChIP-seq in WT and enhancer-deleted RAW cells (Figure 1F). Deletion of E1 enhancer largely reduced H3K27ac in E1, E2, and promoter regions, while deletion of E2 enhancer increased H3K27ac in these regions (Figure 1F), consistent with the changes in gene expression. This was confirmed by ChIP-qPCR (Figure S1L), and it was gene specific, as the enhancer deletions had no effects on the neighboring gene loci (Figure S1M). We continued to knock down GPS2 or SMRT in enhancer-deleted RAW cells to explore the function of the corepressor complex. In E1-deleted cells, knockdown of GPS2 or SMRT had no further effects on *Ccl2* expression (Figures 1G and S1N). This suggests that E2, in the absence of E1, is not capable of driving *Ccl2* transcription despite the loss of co-repressors. In E2-deleted cells, however, knockdown of GPS2 or SMRT further increased *Ccl2* expression. This suggests that E1, even in the absence of E2, is further de-repressed by loss of GPS2 or SMRT. Moreover, in SMRT-knockdown cells, E2 deletion did not further change *Ccl2* expression, suggesting that SMRT participates in E2-mediated repression (Figure S1N). The combined results suggest that E1 acts as the critical enhancer for *Ccl2* gene expression and for repression by GPS2 and SMRT, while E2 is dispensable for *Ccl2* gene expression but instead has features of a silencer those deletion causes de-repression. The chromosomal positions of the corresponding deleted enhancer versus silencer regions along with key TF motifs are outlined in Figure S1O and specified in STAR methods. Hereafter, we refer to E1 as *Ccl2* enhancer (E) and E2 as *Ccl2* silencer (S).

Differential role of enhancer and silencer in transcription complex assembly at the *Ccl2* locus

Gene transcription and H3K27ac are coordinated by TFs, coregulators, and Pol II, which can be mapped by ChIP-seq. However, ChIP-seq alone is not able to identify the primary binding sites of TFs and coregulators, as the cross-linking process fixes protein/DNA complexes in chromatin looping structures within TADs. The individual *Ccl2* E/S deletions therefore represent a feasible tool to map the primary docking sites of TFs and coregulators along with Pol II.

First, we performed ChIP-seq of MED1, CBP, and Pol II in WT and E/S-deleted RAW cells in both LPS and basal condition (Figures 2A and S2). We found that in both conditions, in E-deleted cells the recruitment of these factors was abolished at all linked enhancer, silencer, and promoter regions. In S-deleted cells, however, occupancy of these factors at these regions was not abolished but rather increased (Figures 2A and S2A). These

Top: ChIP-qPCR primer sites at the *Ccl2* locus are labeled as E1 (enhancer 1), E2 (enhancer 2), P (promoter), and C (control). Bottom: the CRISPR-Cas9-mediated deletions are labeled for the distal enhancer as ΔE1.1 and ΔE1.2 and for the proximal enhancer as ΔE2.

(D) Genome Browser tracks of H3K27ac ChIP-seq (basal condition) at the *Ccl2* locus in short hairpin RNA (shRNA)-treated RAW cells to deplete GPS2 or SMRT, in comparison to shGFP as control. Relative H3K27ac changes (percentage) at enhancer E1 were calculated by comparing shGFP (control) versus shGPS2 or shSMRT (n = 2).

(E) qRT-PCR analysis of *Ccl2* mRNA expression in enhancer-deleted RAW cells upon 6 h LPS treatment, compared with vehicle (con) (n = 3). Data significance was determined using unpaired t test.

(F) Genome Browser tracks of H3K27ac ChIP-seq (basal condition) at the *Ccl2* locus in enhancer-deleted RAW cells. Relative H3K27ac changes (percentage) were calculated by comparing WT versus enhancer deletions.

(G) qRT-PCR analysis of *Ccl2* and *Gps2* mRNA expression upon GPS2 depletion in WT and enhancer-deleted RAW cells (n = 3).

One-way ANOVA was used for multiple comparisons. All data are represented as mean ± SEM. *$p < 0.05$, **$p < 0.01$, and ***$p < 0.001$ versus control groups. See also Figure S1.

Please cite this article in press as: Huang et al., The corepressors GPS2 and SMRT control enhancer and silencer remodeling via eRNA transcription during inflammatory activation of macrophages, Molecular Cell (2020), https://doi.org/10.1016/j.molcel.2020.12.040

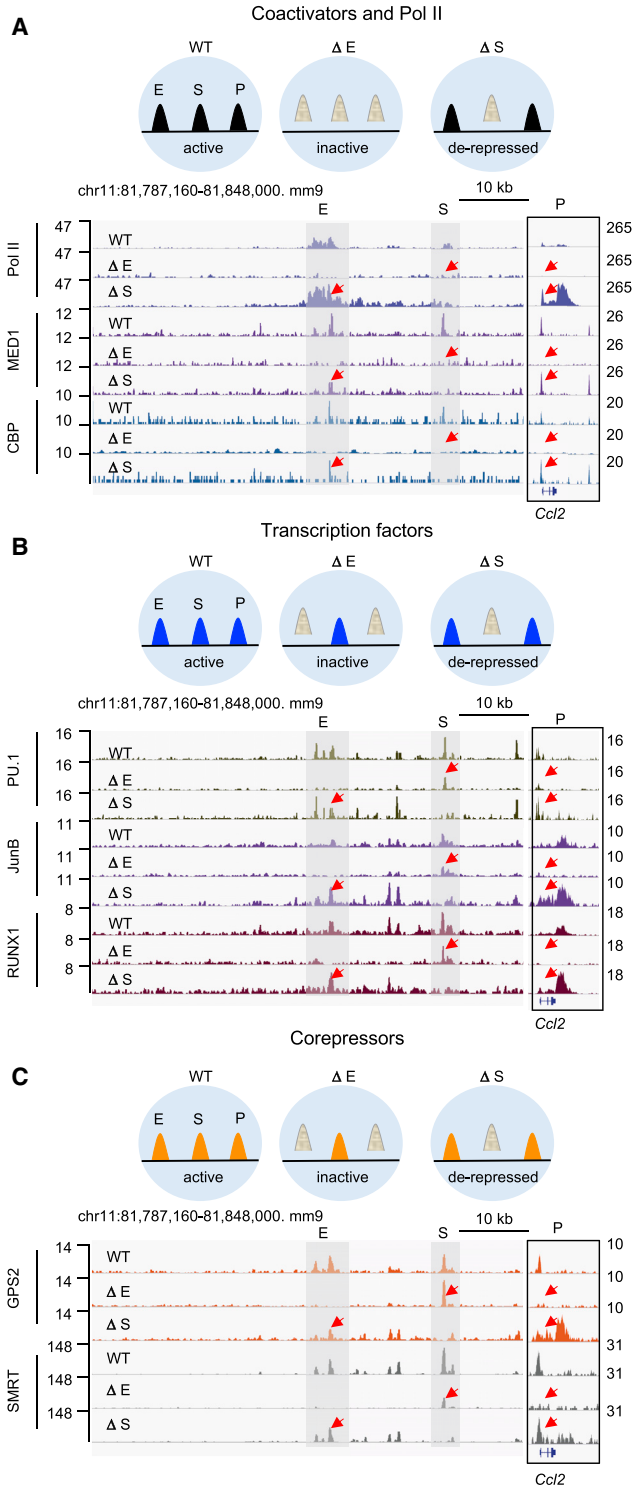

Figure 2. Determination of TF and coregulator recruitment at the *Ccl2* locus

(A–C) Chromatin recruitment upon 2 h LPS treatment was determined using ChIP-seq in WT and enhancer/silencer-deleted RAW cells for (A) Pol II, MED1, and CBP; (B) PU.1, JunB, and RUNX1; and (C) GPS2 and SMRT. Recruitment patterns at the *Ccl2* locus are shown in Genome Browser tracks and schematically highlighted in the pictograms above, emphasizing the distinct effects of each deletion on the recruitment. The y axis represents normalized read counts to the reference mm9 genome. The *Ccl2* enhancer and silencer regions are shadowed in gray. The promoter region was enlarged in the zoom-in window to the right. Peaks that changed upon each deletion are highlighted by red arrows. See also Figure S2.

data are consistent with the changes in H3K27ac and transcription. They indicate that E is the dominant enhancer to assemble the transcriptionally active MED1, CBP, and Pol II complex at the looping structures within the *Ccl2* TAD.

Second, we analyzed the recruitment of relevant macrophage TFs (i.e., highly expressed and motifs enriched at GPS2, MED1, CBP-positive regions), that is, the lineage-determining TFs PU.1, RUNX1, and the signal-responsive AP-1 subunit JunB, in WT and E/S-deleted RAW cells. We found that deletion of E abrogated TF binding at E and promoter, but not at S in both basal and LPS condition (Figures 2B and S2A). This confirmed the E-promoter loop but also suggested that TF binding to S was non-functional, as it was disconnected from coactivator Pol II binding (Figure 2A). In contrast, S deletion led to increased TF binding at E and promoter, which could be a consequence of the increased local concentration of these factors within the S-deleted TAD (Figure 2B). The binding differences of TFs and coactivators were *Ccl2* gene specific, as their binding was not affected at neighboring genes (Figures S2B and S2C). These data suggest that both E and S are the primary docking sites for inflammatory TFs, but only the TFs at E are associated with the promoter.

Third, we analyzed the binding of GPS2 and SMRT in both basal and LPS condition and found distinctive binding patterns. In E-deleted RAW cells, GPS2 was lost at E and promoter but maintained at S, while S deletion increased GPS2 binding at the *Ccl2* promoter (Figures 2C and S2A). Similar to GPS2, SMRT binding at E and promoter was abolished in E-deleted cells, while its binding to E and promoter was not affected in S-deleted cells (Figures 2C and S2A). The recruitment of SMRT and GPS2 at neighboring genes was not affected (Figures S2B and S2C). Strikingly, the binding pattern of GPS2 and SMRT resembles the pattern observed with RUNX1 and JunB (Figures 2B and S2A), suggesting that these TFs might be required for the enhancer recruitment of GPS2 and SMRT but not of CBP and MED1. This is supported by genome-wide motif enrichment analysis, identifying specifically AP-1 motifs to be more frequently enriched in GPS2 and SMRT peaks than in CBP and MED1 peaks (Figures S2D–S2G).

Fourth, we directly compared the recruitment profiles of the above factors in basal versus LPS condition in WT cells in a separate experiment (to minimize batch effects between the comparisons, including variation in cell viability, ChIP efficacy, library amplification, and sequencing). The ChIP-seq data suggest an increase of Pol II, MED1, CBP, PU.1, JunB, and RUNX1 binding in E, S, and promoter regions upon 2 h LPS treatment, while GPS2 and SMRT binding was decreased (Figure S2H). To confirm this and further study the binding dynamics, we performed ChIP-qPCR of GPS2 and JunB at different time points of LPS treatment along with monitoring mRNA expression (Figure S2I). The data reveal unique, in part adverse, chromatin binding dynamics for JunB and GPS2. The dynamics are compatible in the case of JunB, with its transient induction during

Please cite this article in press as: Huang et al., The corepressors GPS2 and SMRT control enhancer and silencer remodeling via eRNA transcription during inflammatory activation of macrophages, Molecular Cell (2020), https://doi.org/10.1016/j.molcel.2020.12.040

inflammatory TLR4 activation (Fonseca et al., 2019), and in the case of GPS2, with the transient corepressor-coactivator switch and feedback mechanisms that terminate transcription despite continued inflammatory signaling (Treuter et al., 2017).

Last, to shed light on features the possibly distinguish the *Ccl2* E and S regions, we mapped H3K27me3, a classic repressive histone modification linked to PRC-mediated chromatin silencing during development (Ngan et al., 2020), along with the mutually exclusive H3K27ac modification linked to activation, in WT and E/S-deleted cells (Figure S2J). Interestingly, H3K27me3 seemed specifically enriched around but not within the S region in WT cells, consistent with S being labeled by H3K27ac. In S-deleted cells, H3K27me3 was largely reduced in E, S, and promoter regions, consistent with the increase of H3K27ac. In contrast, in E-deleted cells, both H3K27me3 and H3K27ac patterns were erased. Collectively, these data depict how TFs, coactivators and corepressors coordinate the enhancer-silencer-promoter-gene interplay at the *Ccl2* locus, they suggest that enhancer and silencer are rather determined by differential factor recruitment than by differential histone marks, and they suggest that corepressors are tightly linked to both enhancer and silencer-bound TFs.

Chromatin dynamics within the *Ccl2* locus upon inflammatory signaling and corepressor depletion

We next explored the role of corepressors in chromatin dynamics within the *Ccl2* TAD. Analysis of published Hi-C data (Link et al., 2018) revealed the TAD covering the mouse *Ccl2* locus, but different signaling conditions were not studied, and the resolution was too low to further specify intra-TAD interactions between enhancers and promoters (Figure S3A). To further dissect these interactions under inflammatory conditions, we performed circular chromosome conformation capture sequencing (4C-seq) (van de Werken et al., 2012), which monitors all genomic regions that interact with a specific region of interest (bait) (Figure 3). In the absence of inflammatory signaling, promoter interactions were detected with S but not with E (Figures 3A, 3B, S3B, and S3C). Strikingly, this situation was reversed upon inflammatory stimulation with LPS (i.e., the S-promoter loop disappeared and instead the E-promoter loop was formed). Furthermore, we found that E and S require the promoter region to form the loops, as deletion of the promoter region abolished all looping structures as well as LPS-induced *Ccl2* gene transcription (Figures 3A, 3B, S3B, and S3C). However, the promoter was not required for TF binding to the distal elements, as deletion of the promoter did not affect PU.1 binding to E and S (Figures S3D and S3E). Furthermore, deletion of either E or S had only marginal effects on promoter interactions of the remaining distal element, supporting the structural independence of enhancer and silencer regions (Figures S3F and S3G).

To address the role of the GPS2 complex in enhancer versus silencer interactions, we performed 4C-seq in corepressor-depleted RAW cells (Figures 3C–3E). We observed that knockdown of either GPS2 or SMRT induced E-promoter interactions, while S interactions with the promoter or E were not affected (Figures 3C–3E and S3H). As H3K27ac and *Ccl2* expression were increased under similar conditions and required E, these data suggest that LPS activation and loss of corepressors have similar effects on the formation of enhancer-selective promoter interactions within the *Ccl2* TAD to regulate gene transcription (Figure 3F), consistent with the TF and coregulator changes both at *Ccl2* locus and genome-wide (Figures S2H and S3K). GPS2 depletion did not alter the chromatin accessibility (ATAC-seq) at the *Ccl2* E, S, and promoter regions but significantly increased MED1 and Pol II binding at E and promoter regions (Figures S3I and S3J). Genome-wide analysis revealed that GPS2 depletion caused increased recruitment of coactivators (MED1 and Pol II) at upregulated genes including *Ccl2* (Figure S3K), while TF binding (JunB and PU.1) was unaffected by GPS2 depletion (Figures S3L and S3M). This confirms that GPS2 controls TF activity but not the access of TFs to chromatin, as it was observed in other contexts (Jakobsson et al., 2009; Huang et al., 2019b).

The *Ccl2* enhancer-transcribed eRNA coordinates CBP-dependent H3K27 acetylation, Pol II recruitment, and enhancer-promoter interactions

Enhancer-transcribed eRNAs correlate with enhancer activity and to the expression of adjacent genes, so we investigated how these events are mechanistically linked at the *Ccl2* locus. We applied global run-on sequencing (GRO-seq) (Kaikkonen et al., 2013) to determine eRNA transcription in RAW cells upon inflammatory LPS stimulation. At the genome-wide level, eRNA expression correlated with gene expression, and eRNA expression plus H3K27ac served as an even better predictor of gene transcription than eRNA expression alone (Figure S4A). At the *Ccl2* locus, eRNA expression was higher at enhancer E than at S (Figure S4B). In addition, enhancer E-derived eRNA (referred to as E eRNA hereafter) expression was increased by LPS or upon depletion of GPS2 or SMRT (Figures 4A and 4B). We next tested E eRNA dynamics in LPS-treated RAW cells (Figure S4C). LPS induction of E eRNA transcription started after 1 h treatment and reached the peak at 2 h. For comparison, *Ccl2* and *Ccl7* mRNA transcription were significantly delayed, with initial induction at 2 h and reaching the peak at 6 or 12 h, respectively (Figure S4C). Interestingly, S deletion further enhanced E eRNA transcription and *Ccl2*/*Ccl7* mRNA expression (Figure S4D), which was consistent with the increased binding of TFs to enhancer E upon deletion of S (Figures 2A and 2B). Also, E eRNA expression did not require the *Ccl2* promoter, as its deletion did not reduce the expression of E eRNA (Figure S4E). This indicates that functional transcription complexes are formed autonomously at *Ccl2* enhancers to trigger eRNA transcription promoter-independently, in contrast to mRNA transcription which is promoter dependent.

We next applied CRISPRi using the dCas9/KRAB repressor system (Thakore et al., 2015) to sterically interfere with enhancer-specific transcription at the *Ccl2* locus (Figure 4C). We constructed specific guide RNAs (gRNAs) directing the dCas9/KRAB repressor to different genomic regions (both positive and negative strands) of E and S. Gene expression analysis revealed that blocking E eRNA transcription reduced *Ccl2* and *Ccl7* mRNA, while blocking S transcription had no significant effect (Figure 4C). To more directly test the role of the E eRNA transcript, without interfering with TF function, we targeted E eRNA using antisense locked nucleic acids (LNA-GapmeRs)

Please cite this article in press as: Huang et al., The corepressors GPS2 and SMRT control enhancer and silencer remodeling via eRNA transcription during inflammatory activation of macrophages, Molecular Cell (2020), https://doi.org/10.1016/j.molcel.2020.12.040

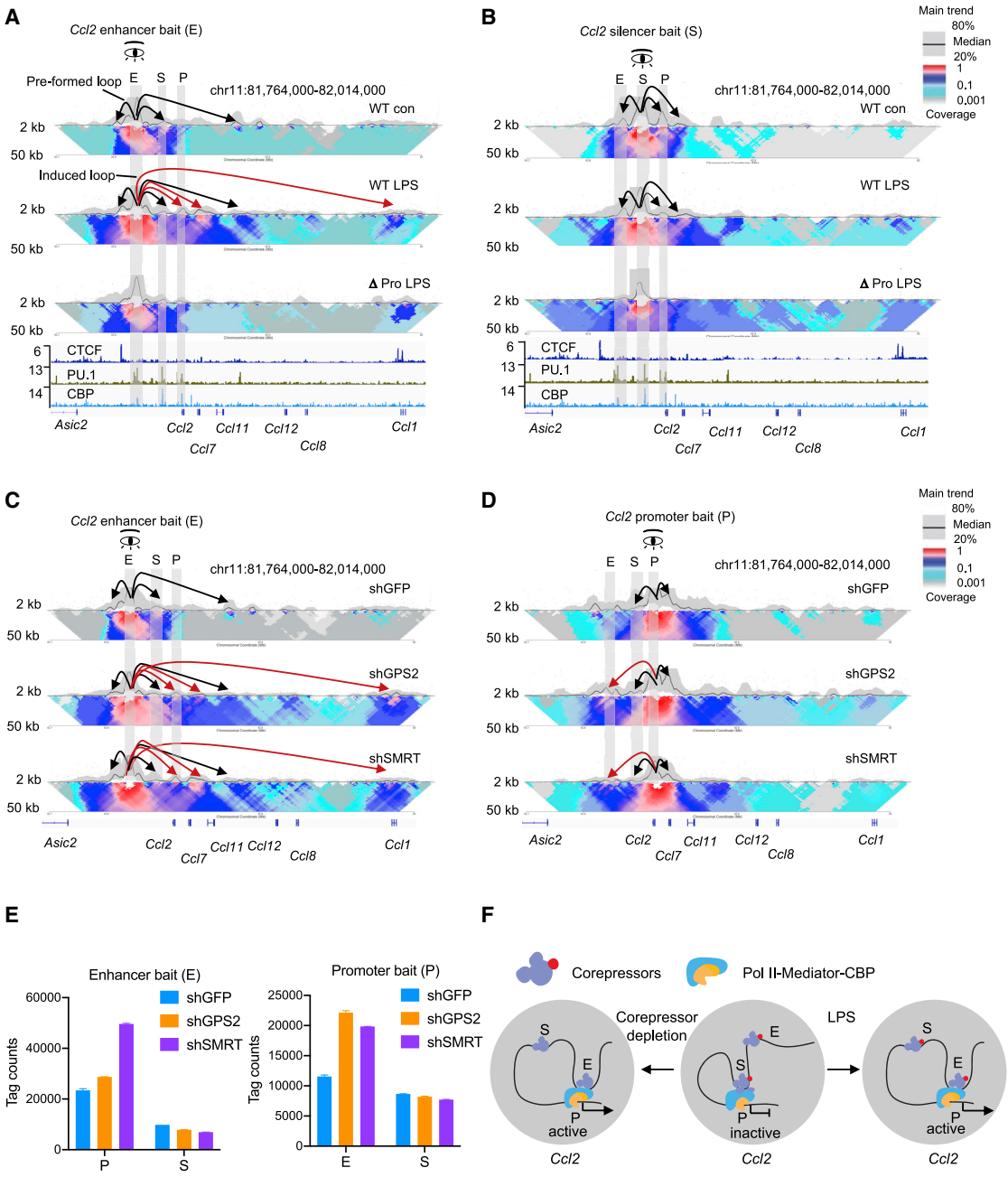

Figure 3. 4C-seq analysis of 3D chromatin structure and enhancer/silencer-promoter interactions at the *Ccl2* locus

(A and B) 4C-seq upon LPS signaling: representative images showing the tracks of 4C-seq-based contact profiles at the *Ccl2* locus using (A) E or (B) S as bait. 4C-seq was performed from untreated WT RAW cells (WT con), WT cells treated with LPS for 2 h (WT LPS), and in promoter-deleted cells treated with LPS for 2 h (ΔPro LPS). The upper panel of 4C-seq data shows the main trend of interaction profiles set to a 250 kb window using 20%–80% percentile values. Interaction frequencies were normalized to the strongest point (bait region). The black line shows the median interaction frequencies. The lower panel shows relative interactions within the 2–50 kb on the basis of a color-coded scale. Red dots indicate strong interactions, and gray dots indicate low interactions. In the lower panel, ChIP-seq data for CTCF (GEO: GSM918726), PU.1, and CBP were used to compare and mark the *Ccl2* enhancers and the CTCF insulating regions (n = 3).

(C and D) 4C-seq upon corepressor depletion: representative images showing tracks of 4C-seq-based contact profiles at the *Ccl2* locus using (C) enhancer E or (D) promoter as bait (n = 2). 4C-seq was performed from control RAW cells (shGFP), GPS2-depleted cells (shGPS2), and SMRT-depleted cells (shSMRT) under basal condition. The induced DNA interactions are highlighted with red arrows and the pre-formed interactions are highlighted with black arrows.

(E) Interaction strength by normalized 4C-seq tag counts for the *Ccl2* promoter bait on *Ccl2* enhancer E and silencer S regions upon depletion of GPS2 or SMRT. The data are represented as mean ± SEM.

(F) Model illustrating the 3D chromatin dynamics and altered enhancer/silencer-promoter interactions at the *Ccl2* locus upon LPS signaling or corepressor depletion. See also Figure S3.

Please cite this article in press as: Huang et al., The corepressors GPS2 and SMRT control enhancer and silencer remodeling via eRNA transcription during inflammatory activation of macrophages, Molecular Cell (2020), https://doi.org/10.1016/j.molcel.2020.12.040

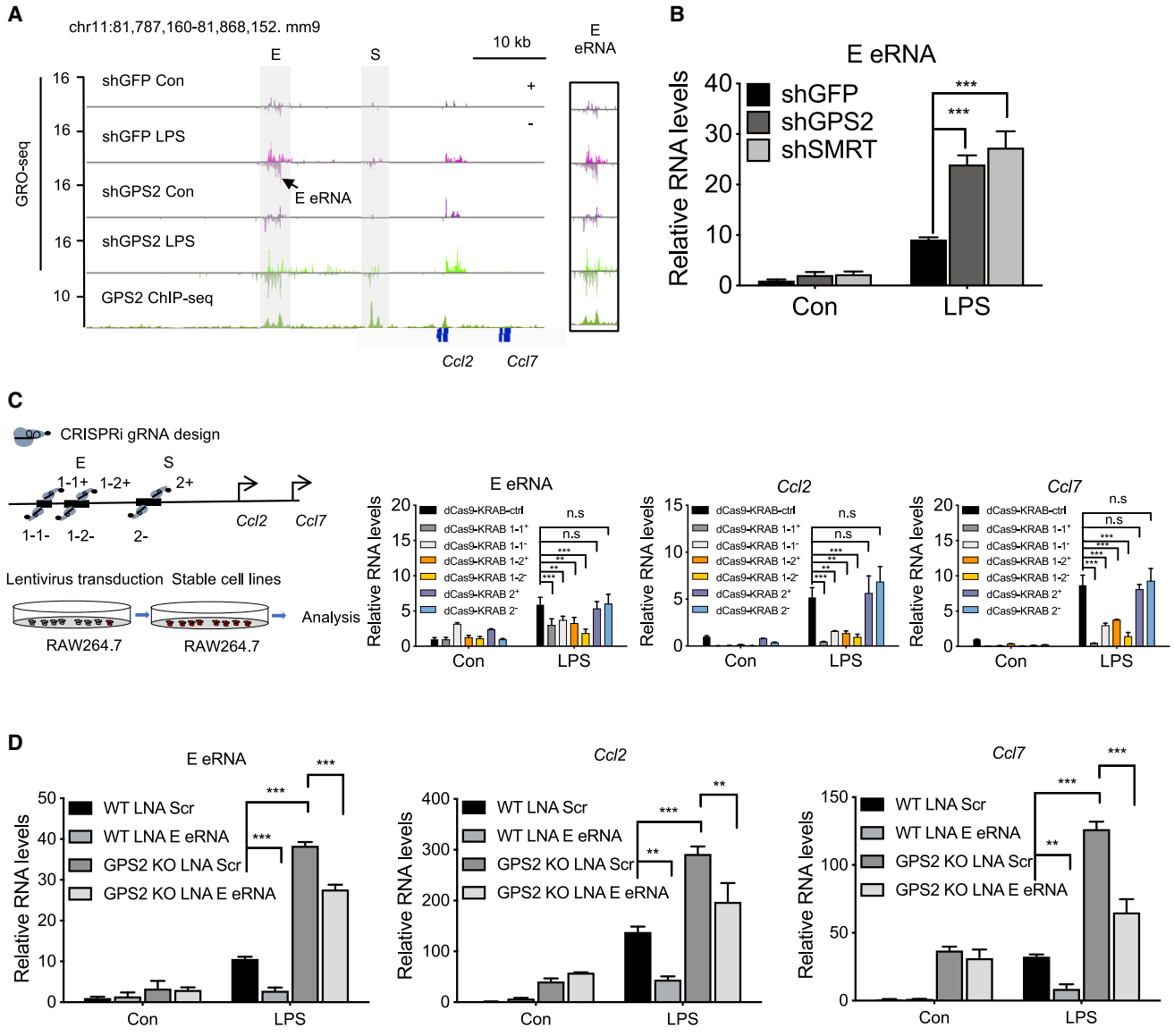

Figure 4. Analysis of eRNA transcription and function at the *Ccl2* locus

(A) Genome Browser tracks of nascent RNA transcription as determined using GRO-seq in control RAW cells (shGFP) and GPS2-depleted cells (shGPS2) upon treatment with vehicle (Con) versus LPS (n = 3). GRO-seq peaks were aligned to GPS2 peaks as determined using ChIP-seq (lower track). The y axis represents normalized read counts to the reference mm9 genome. The *Ccl2* enhancer regions are shadowed in gray, and the E region including transcribed eRNA is enlarged in the zoom-in window to the right.

(B) qRT-PCR analysis of enhancer-transcribed E eRNA expression in control RAW cells (shGFP), GPS2-depleted cells (shGPS2), and SMRT-depleted cells (shSMRT) (n = 3). Data significance was determined using unpaired t test.

(C) Schematic representation of dCas9-KRAB-mediated transcriptional interference via enhancer-selective gRNAs in stably transduced RAW cells (left). qRT-PCR analysis of *Ccl2* E eRNA, *Ccl2*, and *Ccl7* mRNA expression upon 2 h LPS induction in the different dCas9-KRAB gRNA-transduced cell lines (n = 3).

(D) qRT-PCR analysis upon *Ccl2* E eRNA knockdown in WT versus *Gps2*-KO RAW cells with scrambled control LNA (LNA Scr) versus *Ccl2* E eRNA-targeting LNA (LNA E eRNA) upon 2 h LPS induction (n = 3).

One-way ANOVA was used for multiple comparisons. All data are represented as mean ± SEM. *p < 0.05, **p < 0.01, and ***p < 0.001 versus control groups. See also Figure S4.

(Figure 4D). We screened 22 different LNAs and identified 3 functional ones that efficiently reduced E eRNA in LPS-stimulated RAW cells (Figure 4D). Gene expression analysis revealed that LNA-mediated silencing of E eRNA reduced *Ccl2* and *Ccl7* mRNA, consistent with the dCas9/KRAB data but also extending them by suggesting a role of the E eRNA itself (Figure 4D). We also found GPS2-mediated repression of *Ccl2/7* mRNA expression also required E eRNA, as knockdown of E eRNA reduced *Ccl2* and *Ccl7* expression in CRISPR-generated GPS2-KO cells (Figure 4D).

Please cite this article in press as: Huang et al., The corepressors GPS2 and SMRT control enhancer and silencer remodeling via eRNA transcription during inflammatory activation of macrophages, Molecular Cell (2020), https://doi.org/10.1016/j.molcel.2020.12.040

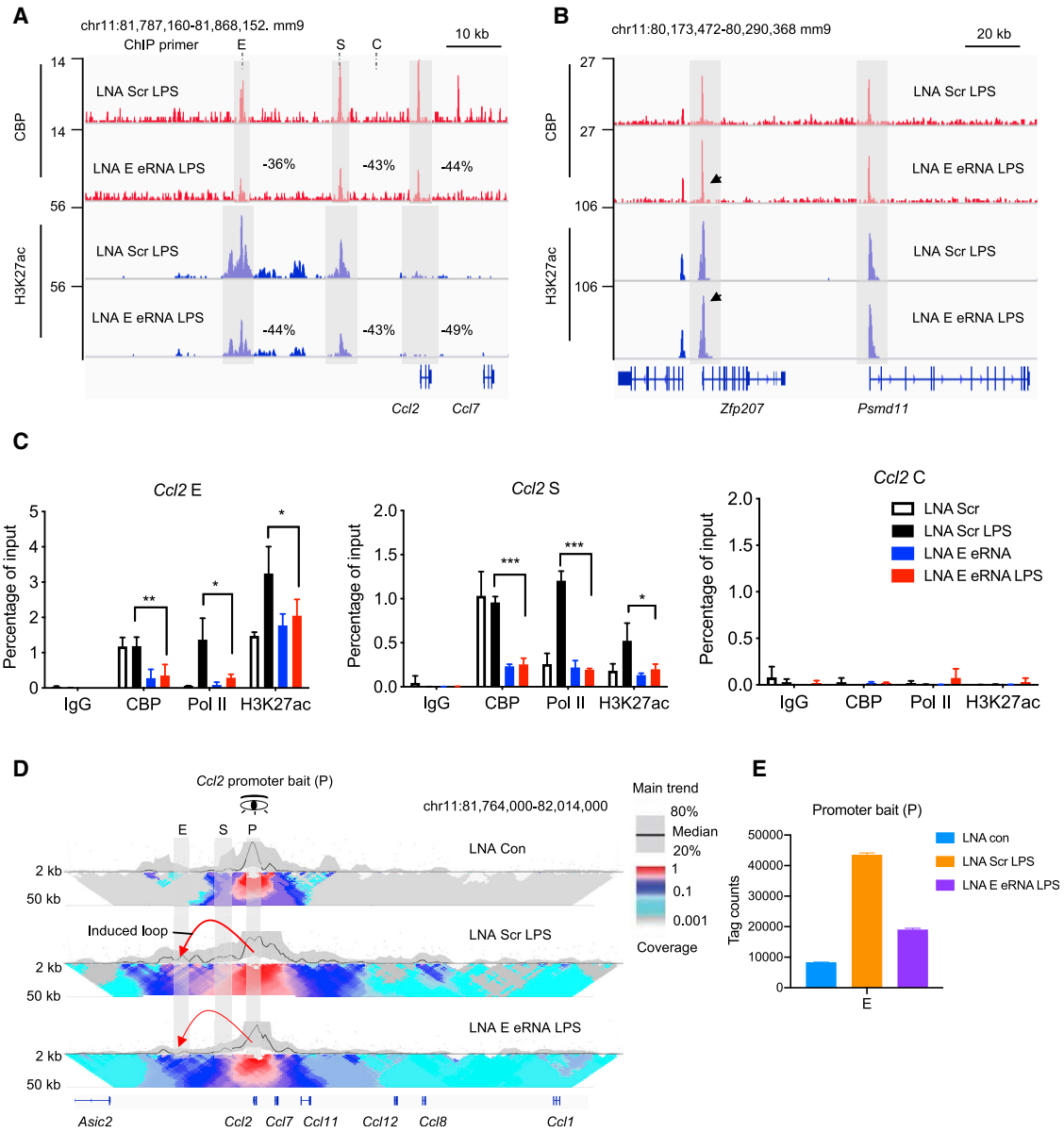

Figure 5. Effects of eRNA depletion on CBP-dependent H3K27 acetylation and chromatin structure at the *Ccl2* locus

(A and B) ChIP-seq for CBP and H3K27ac was performed in RAW cells transfected with scrambled control and E eRNA-specific LNAs and upon treatment with LPS for 2 h. Representative Genome Browser tracks are shown in (A) for the *Ccl2* locus and in (B) for the adjacent *Zfp207* and *Psmd11* loci (outside the *Ccl2* TAD). Relative changes (percentage) at E and S were calculated by comparing LNA control versus *Ccl2* E LNA group.

(C) ChIP-qPCR analysis of CBP and H3K27ac at enhancer E (left), S (middle), and control (right) regions (n = 3). Unpaired t test was used to determine data significance.

(D) Representative 4C-seq tracks using the *Ccl2* promoter as bait showing the interaction profile changes upon LPS induction and E eRNA knockdown (n = 2). The induced DNA interactions are highlighted with red arrows. 4C-seq-derived interaction profiles are presented as in Figures 3A and 3B.

(E) Interaction strength by normalized 4C-seq tag counts for the *Ccl2* promoter bait on *Ccl2* E region. One-way ANOVA was used for multiple comparisons. All data are represented as mean ± SEM. *p < 0.05, **p < 0.01, and ***p < 0.001 LNA Scr LPS versus LNA E eRNA LPS groups.

See also Figure S5.

We further explored the mechanisms of how E eRNA controls *Ccl2* promoter activation and gene transcription. *In vitro*, it has been shown that eRNAs physically bind to CBP and activate its histone acetyltransferase activity, which may link eRNA transcription to H3K27 acetylation during enhancer activation (Bose et al., 2017; Raisner et al., 2018). To test whether this can be recapitulated at the *Ccl2* locus in RAW cells, we performed ChIP-seq of CBP and H3K27ac in WT versus LNA-treated cells (Figure 5A). Indeed, our data indicated that silencing of E eRNA reduced CBP-binding and H3K27ac at E, S, and promoter

Please cite this article in press as: Huang et al., The corepressors GPS2 and SMRT control enhancer and silencer remodeling via eRNA transcription during inflammatory activation of macrophages, Molecular Cell (2020), https://doi.org/10.1016/j.molcel.2020.12.040

(Figure 5A). This effect was restricted to the *Ccl2* TAD, as we observed no changes in the neighboring genes *Zfp207* and *Psmd11* (Figure 5B). The ChIP-seq changes of CBP and H3K27ac were confirmed by ChIP-qPCR analysis (Figure 5C), which additionally revealed that Pol II recruitment at both regions was reduced upon E eRNA silencing. Last, we performed 4C-seq using the *Ccl2* promoter as bait and found that eRNA silencing abolished LPS-induced interactions between promoter and E (Figure 5D). The results were confirmed using E or S as bait (Figures S5A and S5B). Overall, these data support a functional role of the *Ccl2* enhancer E-transcribed eRNA in mediating inflammatory enhancer activation (via CBP-H3K27ac) and sub-TAD formation (via enhancer-promoter looping) to facilitate *Ccl2* mRNA transcription.

Macrophage-specific *Ccl2* eRNA knockdown reduces metaflammation and insulin resistance in *ob/ob* mice

CCL2 is a major and well-studied chemokine that has been associated with adipose tissue macrophage infiltration and insulin resistance in the context of obesity, both in humans and in mouse models (see Introduction). We therefore tested whether *in vivo* depletion of the functional *Ccl2* E eRNA in white adipose tissue (WAT) macrophages of obese (*ob/ob*) mice would have beneficial effects. To achieve this, we generated glucan-encapsulated LNA particles (GeLP) based on the glucan-encapsulated small interfering RNA (siRNA) particle (GeRP) method, which delivers siRNAs (Aouadi et al., 2013; Barreby et al., 2019). Intraperitoneal (i.p.) injection of these particles into 6-week-old *ob/ob* mice leads to macrophage phagocytosis specifically in the WAT, and with the help of the endo-porter peptide the LNAs escape the phagosomes and will silence E eRNA expression within the adipose tissue macrophages (Figure 6A). We observed that upon 10 days of GeLP injection, blood glucose levels of *ob/ob* mice treated with the *Ccl2* E eRNA LNA were significantly lower than in mice treated with scrambled control LNA (Figure 6B). The oral glucose tolerance test (OGTT) revealed improved glucose control upon 10 days of E eRNA silencing (Figure 6C), while baseline OGTT levels were not different between the two groups before treatment (Figure S6A). Furthermore, the total body weight and the weight of different adipose tissue depots were not changed between the two groups upon 10 days of E eRNA silencing (Figures S6B and S6C). Importantly, E eRNA silencing reduced macrophage infiltration of visceral adipose tissue (VAT) by almost 50%, as determined by $F4/80^{+}CD11b^{+}$ fluorescence-activated cell sorting (FACS) analysis (Figure 6D). Consistent with this, expression of the *Ccl2* E eRNA, the *Ccl2* mRNA, and the mRNAs of other inflammatory cytokines were reduced upon E eRNA silencing, both in the stromal vascular fraction (SVF) (Figure 6E) and in $F4/80^{+}$ SVF macrophages (Figure 6F) of the VAT. This reduction seems specifically to occur in the macrophages, as it could not be detected in the whole adipose tissue (mainly adipocytes), that is, VAT (Figure 6G), subcutaneous adipose tissue (SAT) (Figure 6H), and brown adipose tissue (BAT) (Figure S6D), or in the liver (mainly hepatocytes) (Figure S6E). Collectively, these data demonstrate that GeLP-mediated silencing of the *Ccl2* enhancer E-transcribed eRNA in an obese mouse model was effective in reducing *Ccl2* mRNA expression and macrophage inflammation in the WAT and in partially reversing obesity-associated insulin resistance.

DISCUSSION

We systemically investigated the role of the GPS2/SMRT corepressor sub-complex in specifying the function of *cis*-regulatory elements and chromatin remodeling linked to inflammatory gene expression with an emphasis on the *Ccl2* locus, both in cultured macrophages and in obese (*ob/ob*) mice. We identify a role of corepressors in antagonizing enhancer-promoter communication, MED1/Pol II action, CBP-mediated H3K27 acetylation, eRNA transcription, and pro-inflammatory gene expression. Our work thereby helps fill a current knowledge gap, because corepressors are mostly not yet integrated into models of enhancer function, in contrast to TFs and the enhancer-marking coactivators CBP/p300 and MED1.

An intriguing result is that *Ccl2* expression is controlled by non-redundant, functionally distinct *cis*-regulatory regions that seemingly share common features of "active" enhancers, including high H3K27ac, Pol II binding, eRNA transcription, recruitment of shared sets of TFs (PU.1, AP-1, RUNX1), coactivators (MED1, CBP), and corepressors (GPS2, SMRT). The *Ccl2* "super-enhancer" turned out to consist of a major enhancer (E) and a major silencer (S) region. Functional differences became only evident through the combined analysis of deletions (CRISPR-Cas9), inhibition of transcription (CRISPRi), eRNA depletion (antisense LNA GapmeRs), and promoter interactions (4C-seq) along with gene expression analysis. Our results are consistent with recent studies suggesting that silencers are much more common at the genome-wide level than anticipated (Doni Jayavelu et al., 2020; Gisselbrecht et al., 2020; Huang et al., 2019a; Ngan et al., 2020; Pang and Snyder, 2020). Notably, the classic "silencing mark" H3K27me3 (Wiles and Selker, 2017) seems not commonly associated with these silencers. Instead, they are positioned in open chromatin regions and share features with "weak" enhancers (Pang and Snyder, 2020). Key characteristics that distinguish such silencers from enhancers and thereby would allow to predict them have remained enigmatic. Silencers may enrich specific TF repressors, including AP-1 factors (Doni Jayavelu et al., 2020) and corepressors including NCOR (the SMRT homologs core subunit of the HDAC3 complex) (Pang and Snyder, 2020). However, these factors also occupy enhancers, and there is no experimental evidence yet that they are the determinants of silencer function.

Although our study does not identify genome-wide silencers, the insights into the *Ccl2* regulatory landscape have delineated potential silencer features in inflammatory contexts. Regarding AP-1 factors, JunB is found at both silencer and enhancer, and *Ccl2* silencer deletion had a strong de-repression effect upon treatment with TPA (a selective AP-1 activator). AP-1 members are the most abundant TFs at macrophage enhancers, many of which are induced by TLR4 ligands (Fan et al., 2016; Fonseca et al., 2019). Regarding corepressors, although we provide evidence in WT versus SMRT-depleted cells that SMRT is required for the *Ccl2* silencer function, SMRT along with GPS2 also occupies and represses the *Ccl2* enhancer, and most macrophage enhancers genome-wide. Possibly, as corepressors do not

Please cite this article in press as: Huang et al., The corepressors GPS2 and SMRT control enhancer and silencer remodeling via eRNA transcription during inflammatory activation of macrophages, Molecular Cell (2020), https://doi.org/10.1016/j.molcel.2020.12.040

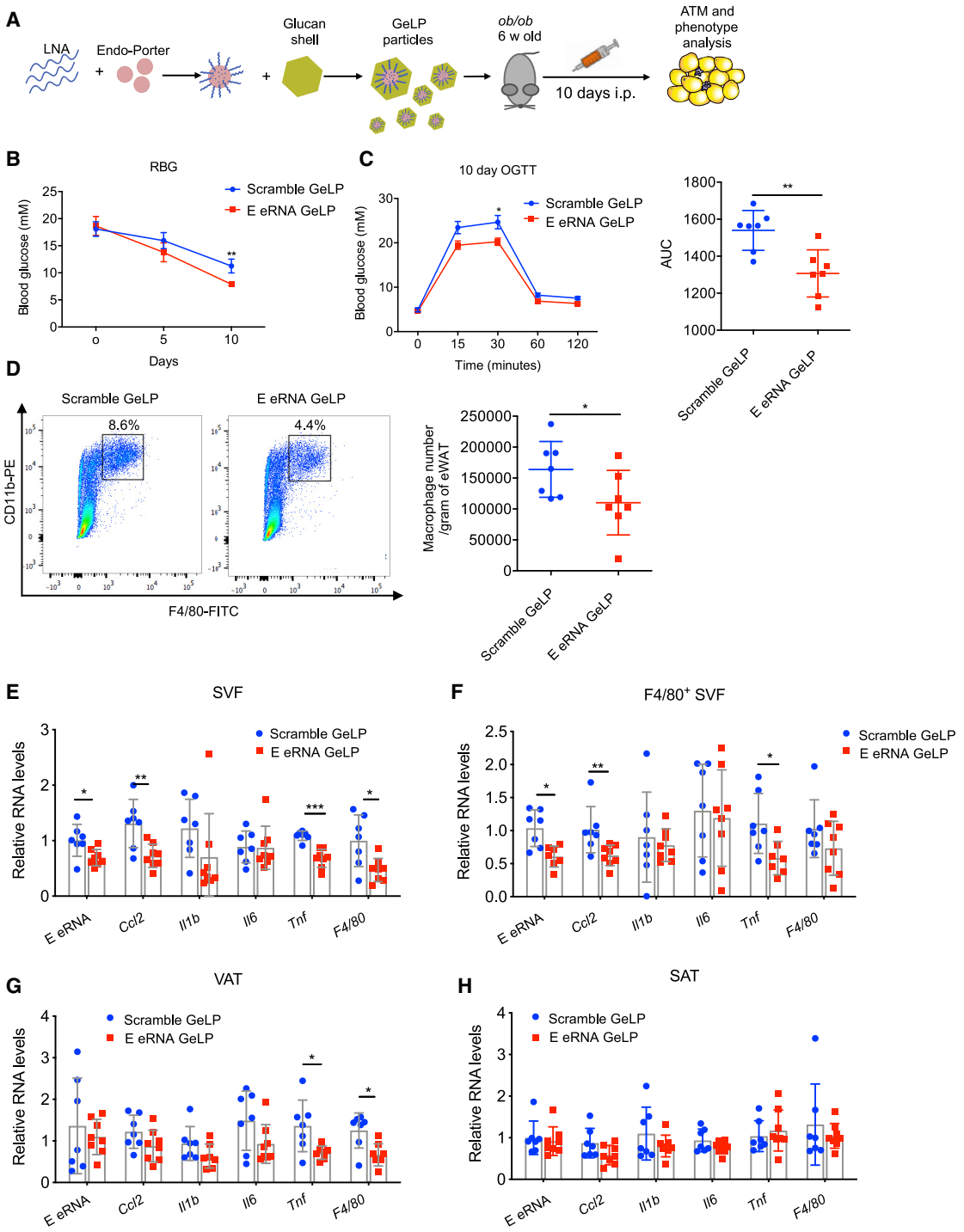

Figure 6. *In vivo* depletion of the *Ccl2* enhancer E-transcribed eRNA in adipose tissue macrophages of *ob/ob* mice

(A) Schematic representation of GeLP-mediated eRNA knockdown in *ob/ob* mice. Mice injected with GeLPs carrying scrambled LNA serve as control group (n = 7), and mice injected with GeLPs carrying *Ccl2* E eRNA selective LNA serve as knockdown group (n = 8).

(B–D) Mice were characterized as follows: (B) random blood glucose (RBG), (C) OGTT, and (D) FACS analysis of F4/80^{+}CD11b^{+} adipose tissue macrophages in visceral adipose tissue (VAT).

(E and F) qRT-PCR analysis of E eRNA and inflammatory genes in (E) stromal vascular fraction (SVF) and (F) F4/80^{+} SVF of VAT.

(G and H) qRT-PCR analysis of E eRNA and inflammatory genes in (G) whole VAT (H) whole subcutaneous adipose tissue (SAT). Unpaired t test was used to determine data significance. All data are represented as mean ± SEM.

*p < 0.05, **p < 0.01, and ***p < 0.001 versus control groups. See also Figure S6.

Please cite this article in press as: Huang et al., The corepressors GPS2 and SMRT control enhancer and silencer remodeling via eRNA transcription during inflammatory activation of macrophages, Molecular Cell (2020), https://doi.org/10.1016/j.molcel.2020.12.040

access DNA directly, their occupancy is a shared feature of silencers and enhancers, but the functional outcome of corepressor occupancy is determined by the underlying dynamic and transient TF networks at silencers versus enhancers. Specifically, the requirement of SMRT but not GPS2 for the *Ccl2* silencer may be explained by the presence of distinct sets of target TFs at silencer versus enhancer, consistent with the assumption that SMRT has a broader TF-binding capacity than GPS (Oberoi et al., 2011; Treuter et al., 2017). Notably, SMRT was originally identified as a "silencing mediator of retinoid and thyroid receptors," which are metabolic sensors and dual repressors/activators within the nuclear receptor TF family (Chen and Evans, 1995). Therefore, our work indicates that the "silencing mediator" concept applies to inflammatory TFs and signaling contexts as well.

Our data support the model that SMRT and GPS2 modulate transcription under basal conditions but also under acute inflammatory conditions. In addition to the ChIP-based data, this is directly evidenced by the elevated LPS induction of inflammatory transcription upon GPS2 or SMRT depletion. This is biologically highly relevant for conditions of acute inflammation (this study) but also for chronic inflammation associated with obesity and type 2 diabetes (metaflammation), conditions that downregulate GPS2 expression (Fan et al., 2016). The combined data suggest that GPS2, along with SMRT within the sub-complex, functions under diverse conditions of inflammatory signaling. This can be understood from assuming a rather dynamic chromatin binding and release behavior of corepressors even under conditions of gene activation, thus expanding the common corepressor-coactivator exchange model (Kuznetsova et al., 2020; Perissi et al., 2010; Treuter et al., 2017).

Given the ongoing debate about whether eRNAs are functional (Kaikkonen and Adelman, 2018), our study supports their role in linking enhancer activity to inflammatory gene expression via modulating CBP-mediated H3K27acetylation (Bose et al., 2017). Specifically, we demonstrate that LNA-mediated knockdown of the *Ccl2* enhancer E-derived eRNA led to reduced H3K27ac at E, S, and promoter, along with reduced *Ccl2* gene expression. Furthermore, GPS2 depletion increases H3K27ac at enhancers *in vivo* (Fan et al., 2016) and *in vitro* (this study). By combining these two findings, we propose a model in which GPS2 and SMRT antagonize eRNA/CBP-dependent H3K27 acetylation at enhancers, presumably independent of HDAC3. Mechanistically, CBP/p300 antagonisms may involve (1) direct competition with CBP/p300 for binding to enhancer-bound TFs, (2) inhibition of eRNA transcription that in turn reduces CBP/p300 HAT activity catalyzing H3K27ac, or (3) interference with CBP/p300 modulation of paused Pol II and elongation (Boija et al., 2017), which may operate at promoter-enhancer loops. The latter mechanism is intriguing as many key inflammatory genes in macrophages are controlled at the level of Pol II pausing and elongation (Heinz et al., 2018; Kaikkonen et al., 2013; Yu et al., 2020). Regarding the question of which TFs are involved, AP-1 family members including c-Jun and JunB are strong candidates: they are direct targets for GPS2 and SMRT (Fan et al., 2016), they are among the most abundant enhancer-enriched TFs upon inflammatory macrophage activation (e.g., LPS/TLR4 signaling) (Fonseca et al., 2019; Glass and Natoli, 2016; Treuter et al., 2017), and they facilitate enhancer-promoter looping upon inflammatory signaling (Phanstiel et al., 2017; Vangala et al., 2020).

Finally, our work has implications for future therapeutic strategies that aim to target enhancers in the context of immune-metabolic disorders. CCL2 is of particular interest, as this macrophage-derived chemokine is a key mediator of metaflammation (Amano et al., 2014; Arner et al., 2012; Bonello et al., 2011; Bot et al., 2017; de Waard et al., 2010; Deshmane et al., 2009; Haringman et al., 2006; Hildebrand et al., 2013; Hotamisligil 2017; Kanda et al., 2006; Katakami et al., 2010; Kawano et al., 2016; Khyzha et al., 2019; Kulyté et al., 2014; Winter et al., 2018; Wolter et al., 2008). We show here that LNA-targeting the *Ccl2* enhancer E-transcribed eRNA in adipose tissue macrophages of *ob/ob* mice could partially reverse metaflammation and insulin resistance. This not only verifies the corepressor-enhancer-eRNA-CCL2 pathway *in vivo*, it also suggests that the selective targeting of inflammatory enhancers/eRNAs in macrophages is possible in mice. As LNA-based therapeutic approaches seem to be safe in humans (Juliano, 2016; Lieberman, 2018; Roux et al., 2017), the feasibility of targeting human enhancer alterations linked to immuno-metabolic diseases (Allum et al., 2019; Liu et al., 2017; Sun et al., 2018) might become clinically relevant in the future.

Limitations of study

First, although in our study the direct function of corepressors at enhancers is well supported by the *Ccl2* locus analysis and by genome-wide data, features of *Ccl2*-related silencers beyond corepressor binding remain poorly understood and require future genome-wide investigations. We imagine that there are unique TF-corepressor networks that need to be scrutinized along with histone marks. Second, to obtain insights into species conservation and relevance for human immuno-metabolic diseases, our analysis must be extended to human monocytes/macrophages. Third, chromatin recruitment of proteins via ChIP-seq must be interpreted with caution, as binding to a particular region does not necessarily mean functionality, and antibodies differ in affinity and specificity making quantitative comparisons difficult. Finally, long-range interactions remain difficult to identify using 4C-seq, so it is not known whether the *Ccl2* enhancer/silencer is additionally engaged in such interactions.

STAR★METHODS

Detailed methods are provided in the online version of this paper and include the following:

- KEY RESOURCES TABLE
- RESOURCE AVAILABILITY
  - Lead contact
  - Materials availability
  - Data and code availability
- EXPERIMENTAL MODEL AND SUBJECT DETAILS
  - Animals
  - Cell Culture Studies
- METHOD DETAILS

Please cite this article in press as: Huang et al., The corepressors GPS2 and SMRT control enhancer and silencer remodeling via eRNA transcription during inflammatory activation of macrophages, Molecular Cell (2020), https://doi.org/10.1016/j.molcel.2020.12.040

CellPress

- Cell cultures and treatments
- ChIP-qPCR and ChIP-seq
- GeLP-mediated eRNA silencing in adipose tissue macrophages of ob/ob mice
- Lentivirus-shRNA-mediated gene knockdown in RAW cells
- Deletion of Ccl2 **enhancer, silencer and promoter** using CRISPR/Cas9
- RNA isolation and RT-qPCR
- GRO-seq
- ATAC-seq
- dCas9–KRAB repression of E eRNA in RAW cells (CRISPRi)
- Flow cytometry
- 4C-seq

- QUANTIFICATION AND STATISTICAL ANALYSIS
  - RNA-seq
  - ChIP-seq
  - GRO-seq
  - ATAC-seq
  - 4C-seq
  - Hi-C
  - Flow cytometry

SUPPLEMENTAL INFORMATION

Supplemental Information can be found online at https://doi.org/10.1016/j.molcel.2020.12.040.

ACKNOWLEDGMENTS

E.T. was supported by grants from the Centre for Innovative Medicine (CIMED) at the Karolinska Institutet, the Swedish Research Council, the Swedish Cancer Society, the Swedish Diabetes Foundation, and the Novo Nordisk Foundation. R.F. was supported by grants from the Swedish Research Council, CIMED, the Novo Nordisk Foundation, and the Karolinska Institutet Research Foundation. J.J. and M.A. were supported by the Strategic Research Program in Diabetes at Karolinska Institutet and the Diabetes Wellness Foundation Sweden. N.V. was supported by the European Union Horizon 20202 (H2020) framework (ERC-EpiFAT 725790). M.U.K. was supported by grants from the European Research Council under the European Union's H2020 research and innovation program (grant 802825), the Academy of Finland, the Sigrid Jusélius Foundation, and the Finnish Foundation for Cardiovascular Research. Z.H. received a doctoral fellowship from the China Scholarship Council (CSC; 201206170053), and N.L. received a doctoral faculty grant (KID) from the Karolinska Institutet. We acknowledge the BEA Core Facility (Karolinska Institutet, Huddinge, Sweden) and the EMBL Genomics Core Facility GeneCore (EMBL, Heidelberg, Germany) for library sequencing. We would like to thank the members of our laboratories and the lecturers of the Spetses Summer Schools in Epigenomics, Nuclear Receptors and Disease (FEBS ALC 17-012, 19-043) for crucial discussions and advice.

AUTHOR CONTRIBUTIONS

Z.H., R.F., and E.T. conceived the study. Z.H. and R.F. performed most experiments, with major input from N.L. and S.G. Z.H., N.L., and A.D. analyzed the sequencing data. C.W. and A.P.B. contributed to the 4C-seq and data analysis. H.N. and M.U.K. performed the GRO-seq and data analysis. T.J. advised and provided tools for the CRISPR-Cas9 experiments. R.F., H.H., M.A., J.J., R.B., and N.V. contributed to the mouse experiments and tissue analysis. Z.H., R.F., and E.T. wrote the manuscript and further edited upon input from all co-authors.

DECLARATION OF INTERESTS

The authors declare no competing interests.

Received: July 1, 2020
Revised: November 20, 2020
Accepted: December 24, 2020
Published: January 26, 2021

REFERENCES

Allum, F., Hedman, A.K., Shao, X., Cheung, W.A., Vijay, J., Guénard, F., Kwan, T., Simon, M.M., Ge, B., Moura, C., et al. (2019). Dissecting features of epigenetic variants underlying cardiometabolic risk using full-resolution epigenome profiling in regulatory elements. Nat. Commun. *10*, 1209.

Amano, S.U., Cohen, J.L., Vangala, P., Tencerova, M., Nicoloro, S.M., Yawe, J.C., Shen, Y., Czech, M.P., and Aouadi, M. (2014). Local proliferation of macrophages contributes to obesity-associated adipose tissue inflammation. Cell Metab. *19*, 162–171.

Andersson, R., and Sandelin, A. (2020). Determinants of enhancer and promoter activities of regulatory elements. Nat. Rev. Genet. *21*, 71–87.

Andersson, R., Gebhard, C., Miguel-Escalada, I., Hoof, I., Bornholdt, J., Boyd, M., Chen, Y., Zhao, X., Schmidl, C., Suzuki, T., et al. (2014). An atlas of active enhancers across human cell types and tissues. Nature *507*, 455–461.

Aouadi, M., Tencerova, M., Vangala, P., Yawe, J.C., Nicoloro, S.M., Amano, S.U., Cohen, J.L., and Czech, M.P. (2013). Gene silencing in adipose tissue macrophages regulates whole-body metabolism in obese mice. Proc. Natl. Acad. Sci. U S A *110*, 8278–8283.

Arner, E., Mejhert, N., Kulyté, A., Balwierz, P.J., Pachkov, M., Cormont, M., Lorente-Cebrián, S., Ehrlund, A., Laurencikiene, J., Hedén, P., et al. (2012). Adipose tissue microRNAs as regulators of CCL2 production in human obesity. Diabetes *61*, 1986–1993.

Barish, G.D., Yu, R.T., Karunasiri, M.S., Becerra, D., Kim, J., Tseng, T.W., Tai, L.J., Leblanc, M., Diehl, C., Cerchietti, L., et al. (2012). The Bcl6-SMRT/NCoR cistrome represses inflammation to attenuate atherosclerosis. Cell Metab. *15*, 554–562.

Barreby, E., Sulen, A., and Aouadi, M. (2019). Glucan-encapsulated siRNA particles (GeRPs) for specific gene silencing in adipose tissue macrophages. Methods Mol. Biol. *1951*, 49–57.

Boija, A., Mahat, D.B., Zare, A., Holmqvist, P.H., Philip, P., Meyers, D.J., Cole, P.A., Lis, J.T., Stenberg, P., and Mannervik, M. (2017). CBP regulates recruitment and release of promoter-proximal RNA polymerase II. Mol. Cell *68*, 491–503.e5.

Bonello, G.B., Pham, M.H., Begum, K., Sigala, J., Sataranatarajan, K., and Mummidi, S. (2011). An evolutionarily conserved TNF-alpha-responsive enhancer in the far upstream region of human CCL2 locus influences its gene expression. J. Immunol. *186*, 7025–7038.

Bose, D.A., Donahue, G., Reinberg, D., Shiekhattar, R., Bonasio, R., and Berger, S.L. (2017). RNA binding to CBP stimulates histone acetylation and transcription. Cell *168*, 135–149.e22.

Bot, I., Ortiz Zacarías, N.V., de Witte, W.E., de Vries, H., van Santbrink, P.J., van der Velden, D., Kröner, M.J., van der Berg, D.J., Stamos, D., de Lange, E.C., et al. (2017). A novel CCR2 antagonist inhibits atherogenesis in apoE deficient mice by achieving high receptor occupancy. Sci. Rep. *7*, 52.

Brown, J.D., Lin, C.Y., Duan, Q., Griffin, G., Federation, A., Paranal, R.M., Bair, S., Newton, G., Lichtman, A., Kung, A., et al. (2014). NF-κB directs dynamic super enhancer formation in inflammation and atherogenesis. Mol. Cell *56*, 219–231.

Buenrostro, J.D., Wu, B., Chang, H.Y., and Greenleaf, W.J. (2015). ATAC-seq: a method for assaying chromatin accessibility genome-wide. Curr. Protoc. Mol. Biol. *109*, 21.29.1–21.29.9.

Chen, J.D., and Evans, R.M. (1995). A transcriptional co-repressor that interacts with nuclear hormone receptors. Nature *377*, 454–457.

Please cite this article in press as: Huang et al., The corepressors GPS2 and SMRT control enhancer and silencer remodeling via eRNA transcription during inflammatory activation of macrophages, Molecular Cell (2020), https://doi.org/10.1016/j.molcel.2020.12.040

Coppo, M., Chinenov, Y., Sacta, M.A., and Rogatsky, I. (2016). The transcriptional coregulator GRIP1 controls macrophage polarization and metabolic homeostasis. Nat. Commun. *7*, 12254.

Cramer, P. (2019). Organization and regulation of gene transcription. Nature *573*, 45–54.

Czimmerer, Z., Daniel, B., Horvath, A., Rückerl, D., Nagy, G., Kiss, M., Peloquin, M., Budai, M.M., Cuaranta-Monroy, I., Simandi, Z., et al. (2018). The transcription factor STAT6 mediates direct repression of inflammatory enhancers and limits activation of alternatively polarized macrophages. Immunity *48*, 75–90.e6.

Daniel, B., Nagy, G., Hah, N., Horvath, A., Czimmerer, Z., Poliska, S., Gyuris, T., Keirsse, J., Gysemans, C., Van Ginderachter, J.A., et al. (2014). The active enhancer network operated by liganded RXR supports angiogenic activity in macrophages. Genes Dev. *28*, 1562–1577.

de Waard, V., Bot, I., de Jager, S.C., Talib, S., Egashira, K., de Vries, M.R., Quax, P.H., Biessen, E.A., and van Berkel, T.J. (2010). Systemic MCP1/CCR2 blockade and leukocyte specific MCP1/CCR2 inhibition affect aortic aneurysm formation differently. Atherosclerosis *211*, 84–89.

Deshmane, S.L., Kremlev, S., Amini, S., and Sawaya, B.E. (2009). Monocyte chemoattractant protein-1 (MCP-1): an overview. J. Interferon Cytokine Res. *29*, 313–326.

Doni Jayavelu, N., Jajodia, A., Mishra, A., and Hawkins, R.D. (2020). Candidate silencer elements for the human and mouse genomes. Nat. Commun. *11*, 1061.

Emmett, M.J., and Lazar, M.A. (2019). Integrative regulation of physiology by histone deacetylase 3. Nat. Rev. Mol. Cell Biol. *20*, 102–115.

Fan, R., Toubal, A., Goñi, S., Drareni, K., Huang, Z., Alzaid, F., Ballaire, R., Ancel, P., Liang, N., Damdimopoulos, A., et al. (2016). Loss of the co-repressor GPS2 sensitizes macrophage activation upon metabolic stress induced by obesity and type 2 diabetes. Nat. Med. *22*, 780–791.

Feng, J., Liu, T., Qin, B., Zhang, Y., and Liu, X.S. (2012). Identifying ChIP-seq enrichment using MACS. Nat. Protoc. *7*, 1728–1740.

Fonseca, G.J., Tao, J., Westin, E.M., Duttke, S.H., Spann, N.J., Strid, T., Shen, Z., Stender, J.D., Sakai, M., Link, V.M., et al. (2019). Diverse motif ensembles specify non-redundant DNA binding activities of AP-1 family members in macrophages. Nat. Commun. *10*, 414.

Gasperini, M., Tome, J.M., and Shendure, J. (2020). Towards a comprehensive catalogue of validated and target-linked human enhancers. Nat. Rev. Genet. *21*, 292–310.

Gisselbrecht, S.S., Palagi, A., Kurland, J.V., Rogers, J.M., Ozadam, H., Zhan, Y., Dekker, J., and Bulyk, M.L. (2020). Transcriptional silencers in Drosophila serve a dual role as transcriptional enhancers in alternate cellular contexts. Mol. Cell *77*, 324–337.e8.

Glass, C.K., and Natoli, G. (2016). Molecular control of activation and priming in macrophages. Nat. Immunol. *17*, 26–33.

Hanssen, L.L.P., Kassouf, M.T., Oudelaar, A.M., Biggs, D., Preece, C., Downes, D.J., Gosden, M., Sharpe, J.A., Sloane-Stanley, J.A., Hughes, J.R., et al. (2017). Tissue-specific CTCF-cohesin-mediated chromatin architecture delimits enhancer interactions and function in vivo. Nat. Cell Biol. *19*, 952–961.

Haringman, J.J., Gerlag, D.M., Smeets, T.J., Baeten, D., van den Bosch, F., Bresnihan, B., Breedveld, F.C., Dinant, H.J., Legay, F., Gram, H., et al. (2006). A randomized controlled trial with an anti-CCL2 (anti-monocyte chemotactic protein 1) monoclonal antibody in patients with rheumatoid arthritis. Arthritis Rheum. *54*, 2387–2392.

Hatzi, K., Jiang, Y., Huang, C., Garrett-Bakelman, F., Gearhart, M.D., Giannopoulou, E.G., Zumbo, P., Kirouac, K., Bhaskara, S., Polo, J.M., et al. (2013). A hybrid mechanism of action for BCL6 in B cells defined by formation of functionally distinct complexes at enhancers and promoters. Cell Rep. *4*, 578–588.

Heinz, S., Benner, C., Spann, N., Bertolino, E., Lin, Y.C., Laslo, P., Cheng, J.X., Murre, C., Singh, H., and Glass, C.K. (2010). Simple combinations of lineage-determining transcription factors prime cis-regulatory elements required for macrophage and B cell identities. Mol. Cell *38*, 576–589.

Heinz, S., Texari, L., Hayes, M.G.B., Urbanowski, M., Chang, M.W., Givarkes, N., Rialdi, A., White, K.M., Albrecht, R.A., Pache, L., et al. (2018). Transcription elongation can affect genome 3D structure. Cell *174*, 1522–1536.e22.

Henriques, T., Scruggs, B.S., Inouye, M.O., Muse, G.W., Williams, L.H., Burkholder, A.B., Lavender, C.A., Fargo, D.C., and Adelman, K. (2018). Widespread transcriptional pausing and elongation control at enhancers. Genes Dev. *32*, 26–41.

Hildebrand, D.G., Alexander, E., Hörber, S., Lehle, S., Obermayer, K., Münck, N.A., Rothfuss, O., Frick, J.S., Morimatsu, M., Schmitz, I., et al. (2013). IκBζ is a transcriptional key regulator of CCL2/MCP-1. J. Immunol. *190*, 4812–4820.

Hotamisligil, G.S. (2017). Inflammation, metaflammation and immunometabolic disorders. Nature *542*, 177–185.

Hsieh, T.S., Cattoglio, C., Slobodyanyuk, E., Hansen, A.S., Rando, O.J., Tjian, R., and Darzacq, X. (2020). Resolving the 3D landscape of transcription-linked mammalian chromatin folding. Mol. Cell *78*, 539–553.e8.

Huang, D., Petrykowska, H.M., Miller, B.F., Elnitski, L., and Ovcharenko, I. (2019a). Identification of human silencers by correlating cross-tissue epigenetic profiles and gene expression. Genome Res. *29*, 657–667.

Huang, Z., Liang, N., Damdimopoulos, A., Fan, R., and Treuter, E. (2019b). G protein pathway suppressor 2 (GPS2) links inflammation and cholesterol efflux by controlling lipopolysaccharide-induced ATP-binding cassette transporter A1 expression in macrophages. FASEB J. *33*, 1631–1643.

Jakobsson, T., Venteclef, N., Toresson, G., Damdimopoulos, A.E., Ehrlund, A., Lou, X., Sanyal, S., Steffensen, K.R., Gustafsson, J.A., and Treuter, E. (2009). GPS2 is required for cholesterol efflux by triggering histone demethylation, LXR recruitment, and coregulator assembly at the ABCG1 locus. Mol. Cell *34*, 510–518.

Jin, F., Li, Y., Dixon, J.R., Selvaraj, S., Ye, Z., Lee, A.Y., Yen, C.A., Schmitt, A.D., Espinoza, C.A., and Ren, B. (2013). A high-resolution map of the three-dimensional chromatin interactome in human cells. Nature *503*, 290–294.

Juliano, R.L. (2016). The delivery of therapeutic oligonucleotides. Nucleic Acids Res. *44*, 6518–6548.

Kaikkonen, M.U., and Adelman, K. (2018). Emerging roles of non-coding RNA transcription. Trends Biochem. Sci. *43*, 654–667.

Kaikkonen, M.U., Spann, N.J., Heinz, S., Romanoski, C.E., Allison, K.A., Stender, J.D., Chun, H.B., Tough, D.F., Prinjha, R.K., Benner, C., and Glass, C.K. (2013). Remodeling of the enhancer landscape during macrophage activation is coupled to enhancer transcription. Mol. Cell *51*, 310–325.

Kanda, H., Tateya, S., Tamori, Y., Kotani, K., Hiasa, K., Kitazawa, R., Kitazawa, S., Miyachi, H., Maeda, S., Egashira, K., and Kasuga, M. (2006). MCP-1 contributes to macrophage infiltration into adipose tissue, insulin resistance, and hepatic steatosis in obesity. J. Clin. Invest. *116*, 1494–1505.

Katakami, N., Matsuhisa, M., Kaneto, H., Matsuoka, T.A., Imamura, K., Ishibashi, F., Kanda, T., Kawai, K., Osonoi, T., Kashiwagi, A., et al. (2010). Monocyte chemoattractant protein-1 (MCP-1) gene polymorphism as a potential risk factor for diabetic retinopathy in Japanese patients with type 2 diabetes. Diabetes Res. Clin. Pract. *89*, e9–e12.

Kawano, Y., Nakae, J., Watanabe, N., Kikuchi, T., Tateya, S., Tamori, Y., Kaneko, M., Abe, T., Onodera, M., and Itoh, H. (2016). Colonic pro-inflammatory macrophages cause insulin resistance in an intestinal Ccl2/Ccr2-dependent manner. Cell Metab. *24*, 295–310.

Khyzha, N., Khor, M., DiStefano, P.V., Wang, L., Matic, L., Hedin, U., Wilson, M.D., Maegdefessel, L., and Fish, J.E. (2019). Regulation of *CCL2* expression in human vascular endothelial cells by a neighboring divergently transcribed long noncoding RNA. Proc. Natl. Acad. Sci. U S A *116*, 16410–16419.

Kim, S., and Shendure, J. (2019). Mechanisms of interplay between transcription factors and the 3D genome. Mol. Cell *76*, 306–319.

Kim, Y.H., Marhon, S.A., Zhang, Y., Steger, D.J., Won, K.J., and Lazar, M.A. (2018). Rev-erbα dynamically modulates chromatin looping to control circadian gene transcription. Science *359*, 1274–1277.

Krietenstein, N., Abraham, S., Venev, S.V., Abdennur, N., Gibcus, J., Hsieh, T.S., Parsi, K.M., Yang, L., Maehr, R., Mirny, L.A., et al. (2020).

Please cite this article in press as: Huang et al., The corepressors GPS2 and SMRT control enhancer and silencer remodeling via eRNA transcription during inflammatory activation of macrophages, Molecular Cell (2020), https://doi.org/10.1016/j.molcel.2020.12.040

Ultrastructural details of mammalian chromosome architecture. Mol. Cell *78*, 554–565.e7.

Krijger, P.H.L., Geeven, G., Bianchi, V., Hilvering, C.R.E., and de Laat, W. (2020). 4C-seq from beginning to end: a detailed protocol for sample preparation and data analysis. Methods *170*, 17–32.

Kulyté, A., Belarbi, Y., Lorente-Cebrián, S., Bambace, C., Arner, E., Daub, C.O., Hedén, P., Rydén, M., Mejhert, N., and Arner, P. (2014). Additive effects of microRNAs and transcription factors on CCL2 production in human white adipose tissue. Diabetes *63*, 1248–1258.

Kuznetsova, T., Prange, K.H.M., Glass, C.K., and de Winther, M.P.J. (2020). Transcriptional and epigenetic regulation of macrophages in atherosclerosis. Nat. Rev. Cardiol. *17*, 216–228.

Lai, F., Damle, S.S., Ling, K.K., and Rigo, F. (2020). Directed RNase H cleavage of nascent transcripts causes transcription termination. Mol. Cell *77*, 1032–1043.e4.

Lam, M.T., Cho, H., Lesch, H.P., Gosselin, D., Heinz, S., Tanaka-Oishi, Y., Benner, C., Kaikkonen, M.U., Kim, A.S., Kosaka, M., et al. (2013). Rev-Erbs repress macrophage gene expression by inhibiting enhancer-directed transcription. Nature *498*, 511–515.

Lee, J.S., and Mendell, J.T. (2020). Antisense-mediated transcript knockdown triggers premature transcription termination. Mol. Cell *77*, 1044–1054.e3.

Li, P., Spann, N.J., Kaikkonen, M.U., Lu, M., Oh, D.Y., Fox, J.N., Bandyopadhyay, G., Talukdar, S., Xu, J., Lagakos, W.S., et al. (2013). NCoR repression of LXRs restricts macrophage biosynthesis of insulin-sensitizing omega 3 fatty acids. Cell *155*, 200–214.

Lieberman, J. (2018). Tapping the RNA world for therapeutics. Nat. Struct. Mol. Biol. *25*, 357–364.

Link, V.M., Duttke, S.H., Chun, H.B., Holtman, I.R., Westin, E., Hoeksema, M.A., Abe, Y., Skola, D., Romanoski, C.E., Tao, J., et al. (2018). Analysis of genetically diverse macrophages reveals local and domain-wide mechanisms that control transcription factor binding and function. Cell *173*, 1796–1809.e17.

Liu, Y., Reynolds, L.M., Ding, J., Hou, L., Lohman, K., Young, T., Cui, W., Huang, Z., Grenier, C., Wan, M., et al. (2017). Blood monocyte transcriptome and epigenome analyses reveal loci associated with human atherosclerosis. Nat. Commun. *8*, 393.

Lovén, J., Hoke, H.A., Lin, C.Y., Lau, A., Orlando, D.A., Vakoc, C.R., Bradner, J.E., Lee, T.I., and Young, R.A. (2013). Selective inhibition of tumor oncogenes by disruption of super-enhancers. Cell *153*, 320–334.

Madsen, J.G.S., Madsen, M.S., Rauch, A., Traynor, S., Van Hauwaert, E.L., Haakonsson, A.K., Javierre, B.M., Hyldahl, M., Fraser, P., and Mandrup, S. (2020). Highly interconnected enhancer communities control lineage-determining genes in human mesenchymal stem cells. Nat. Genet. *52*, 1227–1238.

Mullican, S.E., Gaddis, C.A., Alenghat, T., Nair, M.G., Giacomin, P.R., Everett, L.J., Feng, D., Steger, D.J., Schug, J., Artis, D., and Lazar, M.A. (2011). Histone deacetylase 3 is an epigenomic brake in macrophage alternative activation. Genes Dev. *25*, 2480–2488.

Ngan, C.Y., Wong, C.H., Tjong, H., Wang, W., Goldfeder, R.L., Choi, C., He, H., Gong, L., Lin, J., Urban, B., et al. (2020). Chromatin interaction analyses elucidate the roles of PRC2-bound silencers in mouse development. Nat. Genet. *52*, 264–272.

Oberoi, J., Fairall, L., Watson, P.J., Yang, J.C., Czimmerer, Z., Kampmann, T., Goult, B.T., Greenwood, J.A., Gooch, J.T., Kallenberger, B.C., et al. (2011). Structural basis for the assembly of the SMRT/NCoR core transcriptional repression machinery. Nat. Struct. Mol. Biol. *18*, 177–184.

Osterwalder, M., Barozzi, I., Tissières, V., Fukuda-Yuzawa, Y., Mannion, B.J., Afzal, S.Y., Lee, E.A., Zhu, Y., Plajzer-Frick, I., Pickle, C.S., et al. (2018). Enhancer redundancy provides phenotypic robustness in mammalian development. Nature *554*, 239–243.

Pang, B., and Snyder, M.P. (2020). Systematic identification of silencers in human cells. Nat. Genet. *52*, 254–263.

Papachristou, E.K., Kishore, K., Holding, A.N., Harvey, K., Roumeliotis, T.I., Chilamakuri, C.S.R., Omarjee, S., Chia, K.M., Swarbrick, A., Lim, E., et al. (2018). A quantitative mass spectrometry-based approach to monitor the dynamics of endogenous chromatin-associated protein complexes. Nat. Commun. *9*, 2311.

Partridge, E.C., Chhetri, S.B., Prokop, J.W., Ramaker, R.C., Jansen, C.S., Goh, S.T., Mackiewicz, M., Newberry, K.M., Brandsmeier, L.A., Meadows, S.K., et al. (2020). Occupancy maps of 208 chromatin-associated proteins in one human cell type. Nature *583*, 720–728.

Perissi, V., Jepsen, K., Glass, C.K., and Rosenfeld, M.G. (2010). Deconstructing repression: evolving models of co-repressor action. Nat. Rev. Genet. *11*, 109–123.

Phanstiel, D.H., Van Bortle, K., Spacek, D., Hess, G.T., Shamim, M.S., Machol, I., Love, M.I., Aiden, E.L., Bassik, M.C., and Snyder, M.P. (2017). Static and dynamic DNA loops form AP-1-bound activation hubs during macrophage development. Mol. Cell *67*, 1037–1048.e6.

Raisner, R., Kharbanda, S., Jin, L., Jeng, E., Chan, E., Merchant, M., Haverty, P.M., Bainer, R., Cheung, T., Arnott, D., et al. (2018). Enhancer activity requires CBP/P300 bromodomain-dependent histone H3K27 acetylation. Cell Rep. *24*, 1722–1729.

Ramírez, F., Ryan, D.P., Grüning, B., Bhardwaj, V., Kilpert, F., Richter, A.S., Heyne, S., Dündar, F., and Manke, T. (2016). deepTools2: a next generation web server for deep-sequencing data analysis. Nucleic Acids Res. *44* (W1), W160–W165.

Ren, G., Jin, W., Cui, K., Rodrigez, J., Hu, G., Zhang, Z., Larson, D.R., and Zhao, K. (2017). CTCF-mediated enhancer-promoter interaction is a critical regulator of cell-to-cell variation of gene expression. Mol. Cell *67*, 1049–1058.e6.

Robinson, M.D., McCarthy, D.J., and Smyth, G.K. (2010). edgeR: a Bioconductor package for differential expression analysis of digital gene expression data. Bioinformatics *26*, 139–140.

Robson, M.I., Ringel, A.R., and Mundlos, S. (2019). Regulatory landscaping: how enhancer-promoter communication is sculpted in 3D. Mol. Cell *74*, 1110–1122.

Romanoski, C.E., Link, V.M., Heinz, S., and Glass, C.K. (2015). Exploiting genomics and natural genetic variation to decode macrophage enhancers. Trends Immunol. *36*, 507–518.

Roux, B.T., Lindsay, M.A., and Heward, J.A. (2017). Knockdown of nuclear-located enhancer RNAs and Long ncRNAs using locked nucleic acid gapmeRs. Methods Mol. Biol. *1468*, 11–18.

Russell, D.G., Huang, L., and VanderVen, B.C. (2019). Immunometabolism at the interface between macrophages and pathogens. Nat. Rev. Immunol. *19*, 291–304.

Siersbæk, R., Madsen, J.G.S., Javierre, B.M., Nielsen, R., Bagge, E.K., Cairns, J., Wingett, S.W., Traynor, S., Spivakov, M., Fraser, P., and Mandrup, S. (2017). Dynamic rewiring of promoter-anchored chromatin loops during adipocyte differentiation. Mol. Cell *66*, 420–435.e5.

Sun, W., Yao, S., Tang, J., Liu, S., Chen, J., Deng, D., and Zeng, C. (2018). Integrative analysis of super enhancer SNPs for type 2 diabetes. PLoS ONE *13*, e0192105.

Thakore, P.I., D'Ippolito, A.M., Song, L., Safi, A., Shivakumar, N.K., Kabadi, A.M., Reddy, T.E., Crawford, G.E., and Gersbach, C.A. (2015). Highly specific epigenome editing by CRISPR-Cas9 repressors for silencing of distal regulatory elements. Nat. Methods *12*, 1143–1149.

Treuter, E., Fan, R., Huang, Z., Jakobsson, T., and Venteclef, N. (2017). Transcriptional repression in macrophages-basic mechanisms and alterations in metabolic inflammatory diseases. FEBS Lett. *591*, 2959–2977.

van de Werken, H.J., Landan, G., Holwerda, S.J., Hoichman, M., Klous, P., Chachik, R., Splinter, E., Valdes-Quezada, C., Oz, Y., Bouwman, B.A., et al. (2012). Robust 4C-seq data analysis to screen for regulatory DNA interactions. Nat. Methods *9*, 969–972.

van Steensel, B., and Furlong, E.E.M. (2019). The role of transcription in shaping the spatial organization of the genome. Nat. Rev. Mol. Cell Biol. *20*, 327–337.

Please cite this article in press as: Huang et al., The corepressors GPS2 and SMRT control enhancer and silencer remodeling via eRNA transcription during inflammatory activation of macrophages, Molecular Cell (2020), https://doi.org/10.1016/j.molcel.2020.12.040

Vangala, P., Murphy, R., Quinodoz, S.A., Gellatly, K., McDonel, P., Guttman, M., and Garber, M. (2020). High-resolution mapping of multiway enhancer-promoter interactions regulating pathogen detection. Mol. Cell *80*, 359–373.e8.

Weintraub, A.S., Li, C.H., Zamudio, A.V., Sigova, A.A., Hannett, N.M., Day, D.S., Abraham, B.J., Cohen, M.A., Nabet, B., Buckley, D.L., et al. (2017). YY1 is a structural regulator of enhancer-promoter loops. Cell *171*, 1573–1588.e28.

Wiles, E.T., and Selker, E.U. (2017). H3K27 methylation: a promiscuous repressive chromatin mark. Curr. Opin. Genet. Dev. *43*, 31–37.

Winter, C., Silvestre-Roig, C., Ortega-Gomez, A., Lemnitzer, P., Poelman, H., Schumski, A., Winter, J., Drechsler, M., de Jong, R., Immler, R., et al. (2018). Chrono-pharmacological targeting of the CCL2-CCR2 axis ameliorates atherosclerosis. Cell Metab. *28*, 175–182.e5.

Wolter, S., Doerrie, A., Weber, A., Schneider, H., Hoffmann, E., von der Ohe, J., Bakiri, L., Wagner, E.F., Resch, K., and Kracht, M. (2008). c-Jun controls histone modifications, NF-kappaB recruitment, and RNA polymerase II function to activate the ccl2 gene. Mol. Cell. Biol. *28*, 4407–4423.

Yu, L., Zhang, B., Deochand, D., Sacta, M.A., Coppo, M., Shang, Y., Guo, Z., Zeng, X., Rollins, D.A., Tharmalingam, B., et al. (2020). Negative elongation factor complex enables macrophage inflammatory responses by controlling anti-inflammatory gene expression. Nat. Commun. *11*, 2286.

Please cite this article in press as: Huang et al., The corepressors GPS2 and SMRT control enhancer and silencer remodeling via eRNA transcription during inflammatory activation of macrophages, Molecular Cell (2020), https://doi.org/10.1016/j.molcel.2020.12.040

STAR★METHODS

KEY RESOURCES TABLE

REAGENT or RESOURCE	SOURCE	IDENTIFIER
Antibodies		
Anti-CBP, rabbit monoclonal	Cell Signaling Technology	Cat# (D6C5),7389s; RRID: AB_2616020
Anti-CD11b, mouse monoclonal	Thermo Fisher	Cat# 17-0112-82; RRID: AB_469343
Anti-F4/80, mouse monoclonal	Thermo Fisher	Cat# 25-4801-82; RRID: AB_469653
Anti-GPS2, rabbit polyclonal	This lab	Jakobsson et al., 2009
Anti-H3K27ac, rabbit polyclonal	Abcam	Cat# Ab4729; RRID: AB_2118291
Anti-H3K27me3, rabbit polyclonal	Millipore	Cat# 17-622; RRID: AB_916347
Anti-Jun B, rabbit polyclonal	Santa Cruz Biotechnology	Cat# Sc-46x; RRID: AB_2130022
Anti-MED1, rabbit polyclonal	Bethyl Laboratories	Cat# A300-793A; RRID: AB_577241
Anti-Pol II, mouse monoclonal	BioLegend	Cat# (8WG16),664906; RRID: AB_2565554
Anti-PU.1, rabbit polyclonal	Invitrogen	Cat# PA5-17505; RRID: AB_10989141
Anti-RUNX1, rabbit polyclonal	Abcam	Cat# ab23980; RRID: AB_2184205
Anti-SMRT, rabbit polyclonal	Bethyl Laboratories	Cat# A301-147A; RRID: AB_2149145
Chemicals, peptides, and recombinant proteins		
IL4	Sigma	Cat# SRP3211;
TPA	Sigma	Cat# P8139;
IFNλ	Sigma	Cat# SRP3058;
IL6	Sigma	Cat# I2786;
KLA	Sigma	Cat# 699500P;
TNFα	Sigma	Cat# SRP3177;
LPS	Sigma	Cat# F8666;
FuGENE® HD Transfection Reagent	Promega	Cat# E2311
Disuccinimidyl glutarate (DSG)	VWR	Cat# A7822.0001
Formaldehyde	Thermo Fisher	Cat# 28906
Puromycin	Sigma	Cat# P8833
DNase	Invitrogen	Cat# EN0521
Collagenase II	Thermo Fisher	Cat# 17101015
BSA	Sigma	Cat# 05470
DpnII	NEB	Cat# R0543M
NlaIII	NEB	Cat# R0125L
T4 ligase	NEB	Cat# M0202M
Tn5 transposase	Illumina	Cat #FC-121-1030
DNA Clean and Concentrator-5 Kit	Zymo Research	Cat# D4014
Digitonin	Promega	Cat# G9441
Critical commercial assays		
QIAquick PCR purification kit	QIAGEN	Cat# 28104
Expand long template PCR system	Roche	Cat# 117590600001
Qubit Fluorometric Quantification kit	Thermo Fisher	Cat# Q33238
SMARTer PicoPLEX library preparation kit	Takara	Cat# R400676
SMARTer DNA unique dual index kits	Takara	Cat# R400660-R400663
Clean & Concentrator Capped Zymo-Spin I kit	Zymo Research	Cat# D4013
SYBR Green	KAPA Biosystems	Cat# 07959567001
E.Z.N.A Kit	Omega	Cat# R6834-02

(*Continued on next page*)

Please cite this article in press as: Huang et al., The corepressors GPS2 and SMRT control enhancer and silencer remodeling via eRNA transcription during inflammatory activation of macrophages, Molecular Cell (2020), https://doi.org/10.1016/j.molcel.2020.12.040

Continued

REAGENT or RESOURCE	SOURCE	IDENTIFIER
Superscript III Reverse Transcriptase kit	Invitrogen	Cat# 18080093
ChargeSwitch PCR Clean-Up Kit	Invitrogen	Cat# CS12000
AccuPrime Pfx DNA Polymerase	Invitrogen	Cat# 12344032
Dynabeads M-270 Streptavidin	Invitrogen	Cat# 65305
Deposited data		
NGS data for this study	This paper	GSE130383
BMDM Hi-C data	GEO	GSM2974676
BMDM H3K27ac ChIP-seq	GEO	GSM1631858
BMDM PU.1 ChIP-seq	GEO	GSM1533888
BMDM CTCF ChIP-seq	GEO	GSM918726
BMDM SMRT ChIP-seq	GEO	GSM665925
BMDM GPS2 ChIP-seq	GEO	GSM1631866
BMDM ATAC-seq	GEO	GSM2974654
Experimental models: cell lines		
RAW264.7	ATCC	Cat# TIB-71; RRID: CVCL_0493
HEK293	ATCC	Cat# CRL-1573; RRID: CVCL_0045
Experimental models: organisms/strains		
Mouse: *ob/ob* (JAX Mice Strain)	Charles River Laboratories;	Cat# JAX:000632; RRID: IMSR_JAX:000632
Oligonucleotides		
Primers for *Gapdh*; Forward: ATGGCCTTCCGTGTTCCTA; Reverse: GAAGTCGCAGGAGACAACCT	This paper	N/A
Primers for *Ccl2*; Forward: CAGATGCAGTTAACGCCCCA; Reverse: TGAGCTTGGTGACAAAAACTACAG	This paper	N/A
Primers for *Ccl7*; Forward: GATCTCTGCCACGCTTCTG; Reverse: TGTCTTGAAGATAACAGCTTCCCA	This paper	N/A
Primers for *Tnf*; Forward: AGCCCACGTCGTAGCAAACC; Reverse: GAGGAGCACGTAGTCGGGGC	This paper	N/A
Primers for *Il1b*; Forward: AAATACCTGTGGCCTTGGGC; Reverse: CTTGGGATCCACACTCTCCAG	This paper	N/A
Primers for *Il6*; Forward: GCTGGAGTCACAGAAGGAGTGGC; Reverse: TCTGACCACAGTGAGGAATGTCCA	This paper	N/A
Primers for *F4/80*; Forward: CTTTGGCTATGGGCTTCCAGTC; Reverse: GCAAGGAGGACAGAGTTTATCGTG	This paper	N/A
Primers for *Asic2*; Forward: ACTGTAACTGCCGCATGGTC; Reverse: TTCTGCCAGTAAGCCGAGG	This paper	N/A
Primers for *Gps2*; Forward: ACCAGCTTCTCGGACTCATCTTCT; Reverse: GAGGGTGGGCTGGAGCTCTCT	This paper	N/A
Primers for *Ncor1*; Forward: TGGATCCTGCTGCTGCTTACCT; Reverse: GGCTGCTCTCGTGGGGACAGT	This paper	N/A

(*Continued on next page*)

Please cite this article in press as: Huang et al., The corepressors GPS2 and SMRT control enhancer and silencer remodeling via eRNA transcription during inflammatory activation of macrophages, Molecular Cell (2020), https://doi.org/10.1016/j.molcel.2020.12.040

Continued

REAGENT or RESOURCE	SOURCE	IDENTIFIER
Primers for *Ncor2* ; Forward: GCCCTTAGTCCTAGGTGTGG; Reverse: TTGTACAGAGGCGTGTGGGA	This paper	N/A
Primers for *Junb*; Forward:; ATCCTGCTGGGAGCGGG GAACTGAGGGAAG; Reverse: AGAGTCGTCGTGATAGAAAGGC	This paper	N/A
ChIP primers for *Ccl2* E2 (S); Forward: GGCAGCGAAATGGAAAGAGG; Reverse: GGTCCACAGCAGGATGTACC	This paper	N/A
ChIP primers for *Ccl2* E1(E); Forward: GGTCATGCAAGCCTCTTCCT; Reverse: GCCATTTGTGCAGAAAGCCA	This paper	N/A
ChIP primers for *Ccl2* C; Forward: GGCTTGAACTGTTTGTGACTTT; Reverse: TTTGTACTCTCAAGTCACACATA	This paper	N/A
ChIP primers for *Ccl2* P; Forward: GTCCCTGTCATGCTTCTGGG; Reverse: GGGTGATATGCTGGGAAGGG	This paper	N/A
eRNA primers for *Ccl2* E eRNA ; Forward: AGCCACTGATTTAGCCCCAC; Reverse: GGGGAGCGTGTATATCTCAGG	This paper	N/A
Enhancer deletion oligonucleotides for gRNA 1; Forward: CACCGCTTATTTTCTCCTTTGGAAT; Reverse: AAACATTCCAAAGGAGAAAATAAGC	This paper	N/A
Enhancer deletion oligonucleotides for gRNA 2; Forward: CACCGCCCCTTCAGTCCCTCACATG; Reverse: AAACCATGTGAGGGACTGAAGGGGC	This paper	N/A
Enhancer deletion oligonucleotides for gRNA 3; Forward: CACCGTCAGCACACATACTGACAGA; Reverse: AAACTCTGTCAGTATGTGTGCTGAC	This paper	N/A
Enhancer deletion oligonucleotides for gRNA 4; Forward: CACCGGTATTAACCACAAGAGAGAC; Reverse: AAACGTCTCTCTTGTGGTTAATACC	This paper	N/A
Enhancer deletion oligonucleotides for gRNA 5; Forward: CACCGGAGGCTCCAGGCTTCTCTAG; Reverse: AAACCTAGAGAAGCCTGGAGCCTCC	This paper	N/A
Enhancer deletion oligonucleotides for gRNA 6; Forward: CACCGTGCCATGCCAGGTGTCATGC; Reverse: AAACGCATGACACCTGGCATGGCAC	This paper	N/A

(*Continued on next page*)

Please cite this article in press as: Huang et al., The corepressors GPS2 and SMRT control enhancer and silencer remodeling via eRNA transcription during inflammatory activation of macrophages, Molecular Cell (2020), https://doi.org/10.1016/j.molcel.2020.12.040

Continued

REAGENT or RESOURCE	SOURCE	IDENTIFIER
Enhancer deletion oligonucleotides for gRNA 7; Forward: CACCGCCTGGCCCAGAGTAAGCACT; Reverse: AAACAGTGCTTACTCTGGGCCAGGC	This paper	N/A
Enhancer deletion oligonucleotides for gRNA 8; Forward: CACCGCAGAGCCCTCGGGTGTTTCC; Reverse: AAACGGAAACACCCGAGGGCTCTGC	This paper	N/A
dCas9 oligonucleotides for KRAB-1-1^{+}; Forward: AAACAGGACAGTTACAGTGAGGAG; Reverse: CACCCTCCTCACTGTAACTGTCCT	This paper	N/A
dCas9 oligonucleotides for KRAB-1-1^{-}; Forward: AAACGACTCCAAGTGAGTCTCCAA; Reverse: CACCTTGGAGACTCACTTGGAGTC	This paper	N/A
dCas9 oligonucleotides for KRAB-1-2^{+}; Forward: AAACCAAGAGAGACCGGATCATTA; Reverse: CACCTAATGATCCGGTCTCTCTTG	This paper	N/A
dCas9 oligonucleotides for KRAB-1-2^{-}; Forward: AAACGCACGAGTGTTGCGACAGCA; Reverse: CACCTGCTGTCGCAACACTCGTGC	This paper	N/A
dCas9 oligonucleotides for KRAB-2^{+}; Forward: AAACGAAAGCCTTGCCCAATGTGT; Reverse: CACCACACATTGGGCAAGGCTTTC	This paper	N/A
dCas9 oligonucleotides for KRAB-2^{-}; Forward: AAACACTGGGAGAACAGTTCATTT; Reverse: CACCAAATGAACTGTTCTCCCAGT	This paper	N/A
4C-seq primers for *Ccl2* enhancer bait (E); Forward: GATGAGGCCAAGCAGTAGATC; Reverse: CACTAACTCAGTACCCTAACATG	This paper	N/A
4C-seq primers for *Ccl2* silencer bait (S); Forward: ACCAGACCAATATCTCCTGATC; Reverse: TGCCTTTTGGCAAAAGGACATG	This paper	N/A
4C-seq primers for *Ccl2* promoter bait (P); Forward: GGTGAAACACAGCTCGGATC; Reverse: GTTGGGATCAGAGATACTCATG	This paper	N/A
LNA oligonucleotides for scrambled control ; Forward: AACACGTCTATACGC	This paper	N/A
LNA oligonucleotides for *Ccl2* E eRNA; Forward: TTGGAATTGGAGAACA	This paper	N/A

(*Continued on next page*)

Please cite this article in press as: Huang et al., The corepressors GPS2 and SMRT control enhancer and silencer remodeling via eRNA transcription during inflammatory activation of macrophages, Molecular Cell (2020), https://doi.org/10.1016/j.molcel.2020.12.040

Continued

REAGENT or RESOURCE	SOURCE	IDENTIFIER
shRNA oligonucleotides for GFP; Forward: CCGGGCAAGCTGACCCTGAAGTTCAC TCGAGTGAACTTCAGGGTCAGCTTGC TTTTTG; Reverse:; AATTCAAAAAGCAAG CTGACCCTGAAGTTCACTCGAGTGAAC TTCAGGGTCAGCTTGC	This paper	N/A
shRNA oligonucleotides for GPS2; Forward: CCGGCAGTACCCTCTC TTTGCAGAACTCGAGTTCTGCA AAGAGAGGGTACTGTTTTTG; Reverse: AATTCAAAAACAGTACC CTCTCTTTGCAGAACTCGAGTTCTG CAAAGAGAGGGTACTG	This paper	N/A
shRNA oligonucleotides for SMRT; Forward: CCGGTCCTCGCTGGCC CTCAATTATCTCGAGATAATTGAGGGC CAGCGAGGATTTTTG; Reverse: AATTCAAAAATCCTCGC TGGCCCTCAATTATCTCGAGATAA TTGAGGGCCAGCGAGGA	This paper	N/A
Recombinant DNA		
PX458	Addgene	Cat# 48138
PLKO.1-TRC	Addgene	Cat# 10878
psPAX2	Addgene	Cat# 12260
pMD2.G	Addgene	Cat# 12259
hU6-sgRNA hUbC-dcas9-KRAB-T2a-Puro	Addgene	Cat# 71236
Software and algorithms		
HOMER	http://homer.ucsd.edu/homer/	RRID:SCR_010881
Bowtie	http://bowtie-bio.sourceforge.net/index.shtml	RRID:SCR_005476
Bioconductor	http://www.bioconductor.org/	RRID:SCR_006442
MACS2	https://hbctraining.github.io/Intro-to-ChIPseq/lessons/05_peak_calling_macs.html	RRID:SCR_013291
GraphPad Prism;	https://www.graphpad.com/scientific-software/prism/	RRID:SCR_002798
edgeR	http://bioconductor.org/packages/release/bioc/html/edgeR.html	RRID: SCR_012802
BWA	http://bio-bwa.sourceforge.net/	RRID:SCR_010910
UMass Medical School Flow Cytometry Core Lab, LSRII	https://www.scienceexchange.com/facilities/flow-cytometry-core-lab-umass	RRID:SCR_012630
FlowJo	https://www.flowjo.com/solutions/flowjo	RRID:SCR_008520
4Cseqpipe	http://compgenomics.weizmann.ac.il/tanay/?page_id=367	N/A
HiCExplorer/Galaxy	https://hicexplorer.usegalaxy.eu/	RRID:SCR_006281
Super-Enhancers (ROSE) algorithm	http://younglab.wi.mit.edu/super_enhancer_code.html	RRID:SCR_017390
DESeq2	https://bioconductor.org/packages/release/bioc/html/DESeq2.html	RRID:SCR_015687
RStudio	https://www.rstudio.com/	RRID:SCR_000432
Samtools	https://htslib.org/	RRID:SCR_002105
Deeptools	https://deeptools.readthedocs.io/en/develop/	RRID:SCR_016366
pipe4C-master	https://github.com/deLaatLab/pipe4C	N/A

Please cite this article in press as: Huang et al., The corepressors GPS2 and SMRT control enhancer and silencer remodeling via eRNA transcription during inflammatory activation of macrophages, Molecular Cell (2020), https://doi.org/10.1016/j.molcel.2020.12.040

RESOURCE AVAILABILITY

Lead contact

Further information and requests for resources and reagents should be directed to and will be fulfilled by the Lead Contact, Eckardt Treuter (eckardt.treuter@ki.se).

Materials availability

Mice, antibodies, plasmids and oligonucleotides are listed in the key resources table.

Data and code availability

The published datasets GEO: GSM1631858, GSM1533888, GSM1631866, GSM665925, GSM918726, GSM2974676, GSM2974654 were re-analyzed in this study. RNA-seq, ATAC-seq, ChIP-seq, GRO-seq and 4C-seq data in this study have been deposited in NCBI's Gene Expression Omnibus and are accessible through GEO Series accession number GEO: GSE130383: https://www.ncbi.nlm.nih.gov/geo/query/acc.cgi?acc=GSE130383

EXPERIMENTAL MODEL AND SUBJECT DETAILS

Animals

ob/ob mice (JAX mice strain, stock no. JAX:000632) were obtained from Charles River Laboratories. All mice were maintained at the Center for Comparative Medicine at the Karolinska Institutet and the Karolinska University Hospital (PKL, Huddinge, Sweden), with a 12-h light/dark cycle and free access to diet and water. 6 weeks old male mice were used for the study.

Cell Culture Studies

HEK293 (ATCC, CRL-1573) cells and RAW264.7 (ATCC, TIB-71) were cultured in DMEM supplemented with 10% FBS and antibiotics at 37°C and 5% CO_2.

METHOD DETAILS

Cell cultures and treatments

The mouse RAW264.7 macrophage cell line (ATCC stock no. TIB-71, hereafter referred to as RAW cells) was tested to be free of mycoplasma contamination. RAW cells were cultured in DMEM (GIBCO, 11995073) medium supplemented with 10% heat inactivated FBS (GIBCO, 26140079) and 1% P/S (GIBCO, 15140122). RAW cells were treated with 10 ng/ml LPS (Sigma, L4516) for RNA isolation (6 h) and 100 ng/ml for ChIP-qPCR or ChIP-seq (2 h). The CRISPR/Cas9-mediated GPS2 KO in RAW cells was described in our previous study (Fan et al., 2016). Additional treatments were applied using IL4 (20 ng/ml), TPA (5 nM), IFNλ (100 U/ml), IL6 (20 ng/ml), KLA (10 ng/ml), TNFα (20 ng/ml) for 6 h to induce the *Ccl2* expression in GPS2 KO cells. RAW cells were transfected with Locked Nucleic Acid (LNA) GapmeRs as described previously (Roux et al., 2017) with minor modifications. LNA oligos were ordered from EXIQON with the following sequences: Scrambled control AACACGTCTATACGC, *Ccl2* enhancer (E) eRNA TTGGAATTGGAGAACA. Briefly, 2×10^5 RAW cells were seeded one day before transfection in 24 well plates. The next day, RAW cells were changed with 100 μL antibiotic-free growth medium. 3 μL of 2 μM LNA and 5 μL FuGENE (Promega, E2312) were premixed in 100 μL serum- and antibiotic-free growth medium for 10 min. RAW cells were incubated with the transfection mix in 37°C incubator for 6-15 h (LNA final concentration was 30 nM). 400 μL full growth medium was added to the RAW cells and continued in culture for 24 h. The transfected cells were treated with 10 ng/ml LPS 2 h for RNA extraction. For ChIP-qPCR or ChIP-seq experiments, 2.5×10^6 RAW cells were seeded in 60 mm cell culture plate. Cells were transfected with 30 nM of LNA using FuGENE (Promega, E2311). Cells were treated with 100 ng/ml LPS for 2 h and double crosslinked with 2 mM disuccinimidyl glutarate (DSG) (VWR, A7822.0001) for 30 min, followed by 1% formaldehyde for 10 min (ThermoFisher, 28906). The crosslink reaction was stopped with glycine at a final concentration of 0.125 M for 5 min. The harvested cells were used for ChIP-qPCR or ChIP-seq experiment (in next chapter). The *Ccl2* LNA 4C-seq experiments were performed using 8 plates of 2.5×10^6 RAW cells (in total 2×10^7 cells for two biological replicates) with FuGENE transfection and followed with 4C-seq protocols (see details in the 4C-seq chapter).

ChIP-qPCR and ChIP-seq

ChIP (Chromatin ImmunoPrecipitation)-based experiments were performed as described previously (Fan et al., 2016; Huang et al., 2019b). H3K27ac ChIP-seq were performed using WT and enhancer KO RAW cells (ΔE1.1, ΔE1.2/ΔE and ΔE2/ΔS) without LPS treatment. H3K27ac ChIP-seq were performed in RAW cells using 1 h 100 ng/ml LPS treatment to check the enhancer activation of *Ccl2*. For TF and cofactor ChIP-seq, WT cells, enhancer KO cells (ΔE1.2/ΔE and ΔE2/ΔS), and promoter KO cells were treated for 2 h with/without LPS (100 ng/ml). GFP, GPS2 and SMRT stable knockdown RAW cells were used for H3K27ac ChIP-seq without LPS treatment. CBP, Pol II and H3K27ac ChIP-qPCR and ChIP-seq were performed in *Ccl2* eRNA LNA knockdown cells upon 2 h LPS treatment. Briefly, RAW cells crosslinked with 1% formaldehyde for 10 min for histone modification (H3K27ac) or double crosslinked with 2 mM disuccinimidyl glutarate (DSG) (VWR, A7822.0001) for 30 min, followed by 1% formaldehyde for 10 min. The crosslink reaction

Please cite this article in press as: Huang et al., The corepressors GPS2 and SMRT control enhancer and silencer remodeling via eRNA transcription during inflammatory activation of macrophages, Molecular Cell (2020), https://doi.org/10.1016/j.molcel.2020.12.040

was stopped with glycine at a final concentration of 0.125 M for 5 min. The lysed RAW cell nuclei were sonicated for 30 min (30 s ON/30 s OFF) in Bioruptor Pico (Diagenode, B01060010). Protein A Dynabeads (Invitrogen, 10002D) were incubated with antibodies (specified in KEY RESOURCES TABLE). 2-4 μg antibody was incubated with 100 μg sonicated chromatin DNA sample at 4°C overnight. The next day, beads were washed with wash buffer at least 6 times and followed by reverse-crosslinking at 65°C overnight. The ChIP-ed DNA was purified using Clean & Concentrator Capped Zymo-Spin I (Zymo Research, D4013) kit. For library preparation and sequencing, 1-10 ng of ChIP-ed DNA was processed at the EMBL Genomics Core Facility (Heidelberg, Germany) and BEA Core Facility (Karolinska Institutet, Sweden) using standard protocols, and sequencing was performed in the Illumina HiSeq 2000 (Illumina, 50SE reads) and NextSeq 550 (Illumina, 75SE reads). ChIP-qPCR was performed with SYBR Green (KAPA Biosystems, 07959567001) to validate the ChIP-seq results. Primers for the ChIP–qPCR are listed in the KEY RESOURCES TABLE.

GeLP-mediated eRNA silencing in adipose tissue macrophages of ob/ob mice

Glucan-encapsulated LNA particle (GeLP)-mediated eRNA knockdown was performed in mice following previous protocols (Aouadi et al., 2013; Barreby et al., 2019) with modifications. Briefly, 3 nmol scrambled control LNA (AACACGTCTATACGC) or the LNA targeting the *Ccl2* E eRNA (TTGGAATTGGAGAACA) were mixed with 50 nmol Endo-porter (GeneTools) and 30 mM acetate buffer for 15 min at room temperature. 1 mg glucan particles were added to the mix buffer and incubated for 1 h at room temperature, in dark and without movement. PBS was added to the final volume (200 μl) of delivery dose for one mouse. The final mixed GeLP buffer was sonicated before i.p. injection. *Ob/ob* mice were divided into two groups (n = 7-8) and injected with control versus *Ccl2* enhancer E eRNA-specific GeLPs once every two days for ten days. The random blood glucose (RBG) was tested every day during GeLP injection, and glucose intolerance (OGTT) was tested after then days. After ten days of treatment, mice were sacrificed and adipose tissue macrophages were isolated by FACS. RT-qPCR was performed to determine *Ccl2* and *Ccl7* mRNAs expression, and *Ccl2* E eRNA expression. All mouse procedures were performed in accordance with guidelines approved by the Swedish Ethical Committee (Jordbruksverket) Stockholm.

Lentivirus-shRNA-mediated gene knockdown in RAW cells

The lentivirus-shRNA-mediated knockdown system was described previously (Fan et al., 2016). Lentivirus-shRNAs were constructed for GFP (targeted sequence: GCAAGCTGACCCTGAAGTTCA), GPS2 (targeted sequence: ACCAGCTTCTCGGACTCATCTTCT), and SMRT (targeted sequence: CCAGTGTAAGAACTTCTACTT) and packaged in HEK293FT cells using PLKO.1-TRC (Addgene, 10878), psPAX2 (Addgene, 12260) and pMD2.G (Addgene, 12259) plasmids. 5 MOI viruses were used to infect RAW cells. Stable RAW cells were selected after 48 h virus transduction. Lentivirus-infected cells were selected in full culture medium supplemented with 5 μg/ml puromycin for 7 days. The stable knockdown cells were validated by RT-qPCR before further experiments. Stable GPS2 and SMRT knockdown cells were used for 4C-seq experiments.

Deletion of Ccl2 enhancer, silencer and promoter using CRISPR/Cas9

gRNAs for *Ccl2* enhancer and promoter deletions were designed using the online gRNA design tool DNA Design 2.0 based on GPS2 ChIP-seq data to target the GPS2 peak center chr11 (mm9): 81,818,327-81,818,802 (ΔE1.1); chr11: 81,820,266-81,820,810 (ΔE1.2/ΔE); chr11: 81,836,105-81,836,583 (ΔE2/ΔS) and chr11: 81,848,430-81,848,946 (ΔP). The following sequences of sgRNAs (sgRNA1: CTTATTTTCTCCTTTGGAAT, sgRNA2: CCCCTTCAGTCCCTCACATG, sgRNA3: TCAGCACACATACTGACAGA, sgRNA4: GTATTAACCACAAGAGAGAC, sgRNA5: GAGGCTCCAGGCTTCTCTAG, sgRNA6: TGCCATGCCAGGTGTCATGC, sgRNA7: CCTGGCCCAGAGTAAGCACT, sgRNA8: CAGAGCCCTCGGGTGTTTCC) were inserted into PX458 vector (Addgene, 48138). The transfected GFP-expressing cells were sorted by FACS and followed by serial dilution. The single-cell colonies were validated by sequencing upon TA cloning. PX458 empty vector- transfected and sorted single cell clones were used as negative controls. DNA adjacent to the deleted regions was amplified and sequenced for verification. The deletions were located as follows (mm9): ΔE1.1: chr11:81,818,344-81,818,803, 460bp; ΔE1.2/E: chr11: chr11:81,820,237-81,820,801, 565 bp; and ΔE2/S: chr11:81,836,057-81,836,677, 621bp. TF motif enrichment analysis for the E1.2/E and E2/S core regions was performed with 'findMotifs.pl' by HOMER using default parameters.

RNA isolation and RT-qPCR

Total RNA from cells was isolated using E.Z.N.A Kit (Omega, R6834-02) followed by DNase (Invitrogen, EN0521) treatment according to the manufacturer's instruction. 500 ng of total RNA was used for cDNA synthesis using Superscript III Reverse Transcriptase (Invitrogen, 18080093) with random hexamers. Quantitative transcript analysis was performed using SYBR green (KAPA Biosystems, 07959567001) and run on the Applied Biosystems 7500 Real-time PCR system. Values were normalized using GAPDH as internal control. Primers for the RT–qPCR are listed in the KEY RESOURCES TABLE.

GRO-seq

Global run-on sequencing (GRO-seq) was performed using cell nuclei as previously described (Kaikkonen et al., 2013). Briefly, 15 cm plates of both WT and GPS2 KO or shGFP and shGPS2 RAW cells were treated with vehicle or 100 ng/ml LPS for 1 h and cell nuclei were extracted. The nuclear run-on reaction was performed for 7 min and RNA hydrolysis was allowed to proceed for 10 min. RNA immunoprecipitation was performed by anti-BrdU-conjugated agarose beads (Santa Cruz Biotechnologies). Nascent RNA was

Please cite this article in press as: Huang et al., The corepressors GPS2 and SMRT control enhancer and silencer remodeling via eRNA transcription during inflammatory activation of macrophages, Molecular Cell (2020), https://doi.org/10.1016/j.molcel.2020.12.040

eluted from beads using 400 μl of elution buffer. All GRO-seq library preparations were performed in parallel to avoid batch effects.

ATAC-seq

ATAC-seq (Assay for Transposase-Accessible Chromatin using sequencing) was performed using cell nuclei as previously described (Buenrostro et al., 2015). Briefly, WT and GPS2 KO RAW264.7 cells were seeded with triplicates in the 12 wells plates with 2×10^5 cell number one day before the experiments. Cells were harvested (basal condition), washed with PBS and then resuspended in lysis buffer. Cell nuclei were spun down and transferred into the transposition reaction buffer and incubated at 37 °C for 30 min. Genomic DNA was extracted using QIAGEN MinElute PCR Purification Kit. ATAC-seq libraries were prepared and sequenced on NextSeq 550 (Illumina, 75 SE reads) in the BEA core facility (Karolinska Institutet, Huddinge, Sweden).

dCas9–KRAB repression of E eRNA in RAW cells (CRISPRi)

The dCas9-KRAB repression plasmid pLV hU6-sgRNA hUbC-dCas9-KRAB-T2a-Puro was a gift from Charles Gersbach (Thakore et al., 2015) (Addgene, 71236). gRNAs were selected based on the two enhancer regions of *Ccl2* and cloned into the lentiviral plasmids. The gRNA- containing dCas9-KRAB lentiviruses were packaged in HEK293FT cells and RAW cells were infected and selected. The gRNA target sequences are listed in the Key Resources Table. Stable dCas9-KRAB-gRNA-expressing RAW cells were selected by 5 μg/ml puromycin for 7 days and then used for determining *Ccl2* E eRNA and mRNA expression upon 2 h LPS treatment.

Flow cytometry

Visceral adipose tissues from the *ob/ob* mice were collected and washed in 10 mL DPBS with 0.5% BSA (Sigma Aldrich). Tissues were then cut into small pieces and digested in 3 mL DPBS/BSA supplemented with 4 mg/ml collagenase II (ThermoFisher, 17101015) in 37% shaker (200 rpm) for 30 min. Samples were then filtered using a 100 μm cell strainer (Sigma Aldrich) and washed three times with DPBS/BSA. $1x10^6$ purified cells from each mouse were resuspended in FACS buffer (ThermoFisher) and stained with the indicated fluorescent isotope–conjugated antibodies for 30 min at 4°C in the dark. The antibodies used for FACS included F4/80 (BM8; eBioscience, 25-4801-82, 1:100), CD11b (M1/70; eBioscience, 17-0112-82, 1:300). Cells marked with the antibody were then washed three times with DPBS and fixed in 1% paraformaldehyde before analysis.

4C-seq

Ccl2 enhancer and promoter loops were characterized using chromosome conformation capture (3C) and high-throughput sequencing (4C-seq) as described previously (van de Werken et al., 2012) with slight modifications. In brief, RAW cells were cross-linked with 2% formaldehyde for 10 min and the reaction was stopped with 0.125 M glycine. Cells were counted and 10^7 cells were distributed per tube. WT or LNA control cells, CRISPR KO cells and *Ccl2* E1/E eRNA knockdown cells were re-suspended with 10 mL lysis buffer containing 50 mM Tris-HCl, 150 mM NaCl, 5 mM EDTA, 0.5% NP-40, 1% TX-100, for 10 min. Nuclei were re-suspended into 440 μL Milli-Q water and 60 μL of digestion buffer (15 μL 10% SDS and 75 μL 20% Triton X-100) was added. The cell lysis mixture was then incubated at 37°C for 2 h in the shaker (900 RPM). 200U DpnII (NEB, R0543M) was added into the mixture three times. The lysis mixture was then incubated in the shaker overnight. The reaction mix was inactivated after overnight digestion by incubating at 65°C for 20 min. The samples were then transferred to 50 mL Falcon tubes with 700 μL ligation buffer and 5.5 mL Milli-Q water. The samples were then supplemented with 100 U T4 ligase (NEB, M0202M) and incubated overnight at room temperature. After that, samples were de-crosslinked at 65°C for 12 h. The ligated DNA was then purified by phenol-chloroform method, and further digested with NlaIII (NEB, R0125L) at 37°C overnight. The restriction enzyme was then inactivated for 20 min at 65°C. The DNA was further ligated at room temperature overnight. After the second ligation, the DNA was purified by QIAquick PCR purification kit (QIAGEN, 28104). The 4C library was amplified using *Ccl2* 4C bait primers (provided in the Key Resources Table) by expand long template PCR system (Roche, 117590600001). The PCR products were purified by QIAquick PCR purification kit. The DNA concentration was measured by Qubit Fluorometric Quantification kit (ThermoFisher, Q33238). 10 ng of DNA was used for the high-throughput sequencing library preparation. The library was prepared by SMARTer PicoPLEX library preparation kits (Takara, R400676) and SMARTer DNA unique dual index kits (Takara, R400661). The purified DNA library mix was sequenced on NextSeq 550 (Illumina, 75 SE reads) in BEA Core Facility (Karolinska Institutet, Huddinge, Sweden).

QUANTIFICATION AND STATISTICAL ANALYSIS

All replicate experiments were performed at least two times. ChIP-seq samples which had one biological replicate were confirmed by ChIP-qPCR at the specific target gene locus. D'Agostino and Pearson normality test were used to determine the normal distribution. All statistical tests were performed using GraphPad Prism 6.0b (GraphPad Software, Inc., La Jolla, CA), and all data were represented as mean ± s.e.m. Statistical tests were assessed after confirming that the data met appropriate assumptions (normality, homogeneous variance, and independent sampling). Gaussian distribution was tested using the Kolmogorov–Smirnov test. Group comparisons were assessed with Student's t test to compare two groups, and one-way ANOVA test followed by Tukey's or Dunnett's post hoc test for multiple comparisons as appropriate. All statistical tests were two-tailed, and $p < 0.05$ was defined as significant. No statistical methods were used to predetermine sample size. No samples or animals were excluded from the analyses.

Please cite this article in press as: Huang et al., The corepressors GPS2 and SMRT control enhancer and silencer remodeling via eRNA transcription during inflammatory activation of macrophages, Molecular Cell (2020), https://doi.org/10.1016/j.molcel.2020.12.040

CellPress

RNA-seq

We further analyzed our own published GPS2 KO RNA-seq data from RAW cells (Huang et al., 2019b). Data were aligned to the mouse mm9 genome by using HISAT2. Read counts were imported by HOMER and analyzed using analyzeRepeats with the option rna and parameters -noadj -condenseGenes and -count exons for four replicates per condition. Differential gene expression analysis was performed with DESeq2 using HOMER's getDiffExpression.pl using default parameter. Transcripts with an adjusted p value < 0.05 were considered as differentially expressed genes. The tag counts were plotted by -rpkm for GPS2 KO significantly changed genes in both basal and LPS conditions.

ChIP-seq

Public ChIP-seq data were obtained from the Gene Expression Omnibus (GEO) database (H3K27ac: GSM1631858, PU.1: GSM1533888, CTCF: GSM918726, SMRT: GSM665925, GPS2: GSM1631866, ATAC-seq: GSM2974654) and aligned to the NCBI37/mm9 version of the mouse reference genome. Sequencing files (FASTQ files) were aligned to the NCBI37/mm9 version of the mouse reference genome using Bowtie2 on the Uppsala Multidisciplinary Centre for Advanced Computational Science (UPPMAX) under project SNIC2018/8-122. Sequencing tags were read and imported to the HOMER (Hypergeometric Optimization of Motif EnRichment, http://homer.ucsd.edu/homer) package (Heinz et al., 2010). Peaks were identified using HOMER with default settings, and peak overlap was calculated by merging together all individual peak files for every experiment. The TF motif search was done in Homer by default settings. The statistical comparison of differential peak tag counts was performed using DEseq2 packages in R. Peaks with the adjusted p value < 0.05 were considered as differentially changed peaks. GPS2, MED1, CBP super-enhancer calling was done using the Rank Ordering of Super-Enhancers (ROSE) algorithm (Lovén et al., 2013). GPS2 ChIP-seq data in SMRT knockdown cells were further plotted using DeepTools (Ramírez et al., 2016).

GRO-seq

GRO-seq analysis of genome-wide gene expression was performed with HOMER (Heinz et al., 2010) followed by edgeR. Briefly, the sequencing reads were first trimmed to remove the low-quality reads, adapters and the poly-A sequences. The remaining reads were then aligned to mouse mm9 genome using bwa. For the genome browser visualization, bedGraph files were generated separately for plus and minus DNA strands. The minus strands were presented as negative values in the genome browser. Both gene body and intergenic transcription levels were quantified using HOMER analyzeRepeats.pl in each file. The comparison of differential tag counts in the gene bodies and intergenic regions, and the statistical analysis for differential expression, was performed using the edgeR (Robinson et al., 2010) package in R. Transcripts with an adjusted p value < 0.05 were considered as differentially expressed.

ATAC-seq

The paired-end FASTQ data was aligned to mice mm9 genome using Bowtie2. The ATAC-seq peak calling was done using MACS2 and ENCODE ATAC-seq pipeline (Feng et al., 2012). The statistical analysis for differential expression was further performed using the edgeR. Peaks changes with an adjusted p value < 0.05 were considered as differentially peaks.

4C-seq

The paired-end FASTQ data analysis was performed by the standard 4Cseqpipe protocol (van de Werken et al., 2012). The primer sequences were trimmed from the raw reads. The trimmed reads were mapped to the reference fragmented genome. The contact intensity was normalized by the fragment counts. The cis-interacting DNA contact profiles around the baits were plotted in the same chromosome window. Results from different groups were normalized to the same read counts to compare the significance. Further downstream analysis was performed to obtain the detailed tag counts using Pipe4C-master (Krijger et al., 2020). The FASTQ data were trimmed by bait primers and aligned to the mouse mm9 genome. Aligned bam files were then converted to .wig files by using 10^6 tags as normalize factor. Tag counts were extracted from wig files by using E1/E (chr11:81816382-81822382), E2/S (chr11:81834000-81839000), and promoter (chr11:81846000-81852000) coordinates, respectively, and then visualized in GraphPad software.

Hi-C

The public BMDM Hi-C data GSM2974676 (Link et al., 2018) was obtained from GEO database. The paired-end FASTQ data was mapped on Galaxy/HiCExplorer using BWA-MEM tool. hicBuildMatrix tool was used to build the Hi-C contacts. The corrected Hi-C matrix was plotted using 50 kb and 5 kb contact matrix. The Hi-C contacts were integrated with the ChIP-seq data using the hicPlotTAD tool.

Flow cytometry

Samples were analyzed in a LSRII cytometer (Becton Dickinson) using FACS Diva (BD Biosciences) and FlowJo (Tree Star) softwares.